Cascades and Collapses, Great Walls and Forbidden Cities: Infinite Towers of Metastable Vacua in Supersymmetric Field Theories

Keith R. Dienes and Brooks Thomas
Department of Physics, University of Arizona, Tucson, AZ 85721 USA

In this paper, we present a series of supersymmetric models exhibiting an entirely new vacuum structure: towers of metastable vacua with higher and higher energies. As the number of vacua grows towards infinity, the energy of the highest vacuum remains fixed while the energy of the true ground state tends towards zero. We study the instanton-induced tunneling dynamics associated with such vacuum towers, and find that many distinct decay patterns along the tower are possible: these include not only regions of vacua experiencing direct collapses and/or tumbling cascades, but also other regions of vacua whose stability is protected by "great walls" as well as regions of vacua populating "forbidden cities" into which tunnelling cannot occur. We also discuss possible applications of this setup for the cosmological-constant problem, for studies of the string landscape, for supersymmetry breaking, and for Z' phenomenology. Finally, we point out that a limiting case of our setup yields theories with yet another new vacuum structure: infinite numbers of degenerate vacua. As a result, the true ground states of such theories are Bloch waves, with energy eigenvalues approximating a continuum and giving rise to a vacuum "band" structure.

I. INTRODUCTION

The vacuum structure of any physical theory plays a significant and often crucial role in determining the physical properties of that theory. Indeed, critical issues such as the presence or absence of spontaneous symmetry breaking often depend entirely on the vacuum structure of the theory in question.

Likewise, it may happen that a given model contains not only a true ground state, but also a metastable vacuum state above it. Such models are also of considerable interest, for even when the true ground state preserves the apparent symmetries of a model, the physical properties associated with the metastable vacua can often differ markedly from those of the ground state. In such situations, the resulting phenomenology of the model might be determined by the properties of a metastable vacuum rather than by those of the true ground state.

In recent years, models containing metastable vacua have captured considered attention. This is true for a variety of reasons. For example, metastable vacua can serve as a tool for breaking supersymmetry [1, 2] in the context of certain supersymmetric non-Abelian gauge theories which are otherwise known to contain supersymmetric ground states. In addition, theories with large numbers of vacua have also been exploited in various ways as a means of addressing the cosmological-constant problem [3, 4, 5, 6] and obtaining de Sitter vacua in string compactifications [7]. Furthermore, the possibility of phase transitions in theories with multiple (meta)stable vacua leads to a number of implications for cosmology.

Such ideas provide ample motivation to investigate whether there might exist relatively simple field theories which give rise to additional, heretofore-unexplored vacuum structures. If so, such structures could potentially provide new ways of addressing a variety of unsolved questions about the universe we inhabit.

In this and a subsequent companion paper [8], we will demonstrate that two new non-trivial vacuum structures are possible in relatively simple supersymmetric field theories. Moreover, as we shall see, the models which give rise to these non-trivial vacuum structures are not esoteric; they are, in fact, simple generalizations of $U(1)$ quiver gauge theories.

- First, we shall demonstrate through an explicit construction that certain supersymmetric field theories can give rise to large (and even infinite) towers of metastable vacua with higher and higher energies. The emergence and analysis of this vacuum structure will be the primary focus of the present work. As we shall see, as the number of vacua grows towards infinity in such models, the energy of the highest vacuum remains fixed while the energy of the true ground state tends towards zero. We shall study the instanton-induced tunneling dynamics associated with such vacuum towers, and find that many distinct decay patterns along the tower are possible: these include not only regions of vacua experiencing direct collapses and/or tumbling cascades, but also other regions of vacua whose stability is protected by "great walls" as well as regions of vacua populating "forbidden cities" into which tunnelling cannot occur. Furthermore, as we shall see, these vacua are phenomenologically distinct from one another in terms of their mass spectra and effective interactions.

- Second, we shall also show that there exists a limiting case of the above construction in which all of these infinite metastable vacua become degenerate, and in which there emerges a shift symmetry relating one vacuum to the next. As a result, the true ground states of such theories are nothing but Bloch waves across these degenerate ground states, with energy eigenvalues approximating a continuum and giving rise to a vacuum "band" structure. In this paper, we will merely sketch how such a

vacuum structure emerges; the complete analysis of such a structure will be the subject of a subsequent companion paper [8].

This paper is organized as follows. In Sect. II, we present the framework on which our model is based. As we shall see, our model is essentially nothing more than an Abelian quiver gauge theory, expanded to allow kinetic mixing between the various $U(1)$ factors. We shall then proceed to discuss the corresponding vacuum structure which emerges from this framework, including all stable vacua and all saddle-point barriers between them. We shall also discuss radiative corrections to this vacuum structure, and demonstrate that these corrections can be kept under control. In Sect. III, we shall then discuss the decay dynamics along these metastable vacuum towers, and examine the different sorts of instanton-induced tunneling decay patterns which are possible. In Sect. IV, we then analyze the particle spectra in each vacuum of the tower, and demonstrate how these spectra evolve as our system tumbles down the vacuum tower. In Sect. V we shift gears briefly, and consider the limiting case of our scenario in which our infinite towers of metastable vacua become an infinite series of degenerate ground states. Thus, in this limit, the true ground states of such theories are Bloch waves. Finally, in Sect. VI, we enumerate the potential physical applications of our vacuum towers, including possible new ideas for the cosmological-constant problem, for studies of the string landscape, and for Z' phenomenology.

We emphasize that our primary goal in both papers is the demonstration that such non-trivial vacuum structures can emerge in relatively simple supersymmetric field theories. Although there exist numerous implications and applications of these ideas (some of which will be discussed in Sect. VI), our primary goal in these papers will be the study of the emergence and properties of these vacuum structures themselves.

II. THE GENERAL FRAMEWORK

We begin by presenting our series of supersymmetric models which give rise to infinite towers of metastable vacua. Specifically, for each $N > 1$, we shall present a model which contains not only a stable vacuum ground state but also a tower of $N-2$ metastable vacua above it. Our model consists of N different $U(1)$ gauge group factors, denoted $U(1)_a$ ($a = 1, ..., N$), as well as $N+1$ different chiral superfields, denoted Φ_i ($i = 1, ..., N+1$). These superfields carry the $U(1)$ charge assignments shown in Table I, and follow the well-known orbifolded "moose" pattern wherein each field Φ_i with $2 \leq i \leq N$ simultaneously carries both a positive unit charge under $U(1)_{i-1}$ and a negative unit charge under $U(1)_i$. By contrast, the fields Φ_1 and Φ_{N+1} sit at the orbifold endpoints of the moose, and are charged only under the corresponding endpoint gauge groups respectively. We shall assume that each $U(1)_a$ gauge field has a corresponding gauge coupling g_a, and for simplicity we shall further assume that $g_a \equiv g$ for all a. Note that the only non-vanishing gauge anomalies inherent in this charge configuration are mixed $U(1)$ anomalies proportional to $\sum_i^{N+1} Q_{ai}^2 Q_{bi}$, which can be canceled by the variant of the Green-Schwarz mechanism [9] discussed in Ref. [10].

	$U(1)_1$	$U(1)_2$	$U(1)_3$	$U(1)_4$	...	$U(1)_{N-1}$	$U(1)_N$
Φ_1	-1	0	0	0	...	0	0
Φ_2	$+1$	-1	0	0	...	0	0
Φ_3	0	$+1$	-1	0	...	0	0
Φ_4	0	0	$+1$	-1	...	0	0
$\vdots$	$\vdots$	$\vdots$	$\vdots$	$\vdots$	$\ddots$	$\vdots$	$\vdots$
Φ_{N-1}	0	0	0	0	...	-1	0
Φ_N	0	0	0	0	...	$+1$	-1
Φ_{N+1}	0	0	0	0	...	0	$+1$

TABLE I: The field content and charge assignments for the chiral superfields in the models under consideration.

To this core model we then add three critical ingredients, each of which is vital for the emergence of our metastable vacuum towers. First, given the field content of each model, we see that the most general superpotential that can be formed in each case consists of a single Wilson-line operator

$$W \;=\; \lambda \prod_{i=1}^{N+1} \Phi_i \;. \tag{1}$$

We shall therefore assume that this operator is turned on for each value of N. Note that the coupling λ has mass dimension $2-N$ and is therefore non-renormalizable for all $N > 2$.

Our second and third ingredients both exploit the Abelian nature of our gauge groups. The second ingredient is to introduce non-zero Fayet-Iliopoulos terms ξ_1 and ξ_N for the "endpoint" gauge groups $U(1)_1$ and $U(1)_N$ respectively. While all of our $U(1)_a$ gauge groups could in principle have corresponding non-zero Fayet-Iliopoulos terms ξ_a, we shall see that turning on only ξ_1 and ξ_N will be sufficient for our purposes. Indeed, we shall prune our model further by taking $\xi_1 = \xi_N \equiv \xi$.

Finally, our third ingredient is a simple one: kinetic mixing [11]. It is well-known that the field strength tensor $F^{\mu\nu}$ for an Abelian gauge group is gauge invariant by itself. Thus, in a theory involving multiple $U(1)$ gauge groups, nothing forbids terms proportional to $F_a^{\mu\nu} F_{b,\mu\nu}$ from appearing as kinetic terms in the Lagrangian, where $a \neq b$. Similarly, in a supersymmetric model, mixing between the field-strength superfields W_α^a is permitted, whereupon the gauge-kinetic part of the Lagrangian may take the generic form [12]

$$\mathcal{L} \;\ni\; \frac{1}{32} \int d^2\theta \;\; W_{a\alpha}\, X_{ab}\, W_b^\alpha \tag{2}$$

with a general (symmetric) kinetic-mixing matrix X_{ab}:

$$X_{ab} \equiv \begin{pmatrix} 1 & -\chi_{12} & -\chi_{13} & \dots & -\chi_{1N} \\ -\chi_{12} & 1 & -\chi_{23} & \dots & -\chi_{2N} \\ -\chi_{13} & -\chi_{23} & 1 & \dots & -\chi_{3N} \\ \vdots & \vdots & \vdots & \ddots & \vdots \\ -\chi_{1N} & -\chi_{2N} & -\chi_{3N} & \dots & 1 \end{pmatrix} . \quad (3)$$

As long as X_{ab} is non-singular, with positive real eigenvalues, there exists a matrix M_{ab} which transforms the $U(1)$ gauge groups into a basis in which their gauge-kinetic terms are diagonal and canonically normalized. Specifically, one can write $W_a^T X_{ab} W_b = (\hat{W}_a)^T (\hat{W}_a)$ where $\hat{W}_a \equiv M_{ab} W_b$. In general, such a matrix M takes the form $M = \mathcal{S}\mathcal{O}$ where $\mathcal{S}$ is a diagonal rescaling matrix whose entries are the square roots of the eigenvalues of X and where $\mathcal{O}$ is an orthogonal rotation matrix diagonalizing X. After this diagonalization process, the new $U(1)_a$ charge assignments $\hat{Q}_{ai}$ for our fields Φ_i and the new Fayet-Iliopoulos parameters $\hat{\xi}_a$ for our gauge groups $U(1)_a$ are given in terms of the quantities Q_{ai} and ξ_a in the original basis:

$$\begin{aligned} \hat{Q}_{ai} &= [(M^{-1})^T]_{ab}\, Q_{bi} \\ \hat{\xi}_a &= [(M^{-1})^T]_{ab}\, \xi_b \ . \end{aligned} \quad (4)$$

In this vein, it is important to note that the matrix M corresponding to each kinetic-mixing matrix X is not unique. Any matrix of the form $M' = VM$, where V is an orthogonal matrix, also yields the correct normalization for the gauge-kinetic terms. Different choices for V correspond to different orthogonal choices for the final basis of $U(1)$'s. Ultimately, the physics is insensitive to which basis is chosen. By contrast, the rescaling matrix $\mathcal{S}$ is unique, and it is this matrix which carries the physical effects of kinetic mixing.

In general, any of the χ_{ab} parameters in Eq. (3) may be non-zero. However, it will be sufficient for our purposes to restrict our attention to the case in which only "nearest-neighbor" $U(1)$'s experience mixing. Thus we shall assume that $\chi_{ab} \neq 0$ if and only if $b = a + 1$. For simplicity, we shall further assume that all non-zero χ_{ab} are equal, so that $\chi_{ab} = \chi \delta_{a+1,b}$. While more general kinetic-mixing parameters may be chosen, we shall see that these simplifications enable us to expose the existence of our metastable vacuum towers most directly.

Needless to say, it would have been possible to construct our models entirely without kinetic mixing by postulating highly non-trivial choices for $\hat{Q}_{ai}$ and $\hat{\xi}_a$ right from the beginning. However, we have found that it is easier to begin with the simpler assignments Q_{ai} shown in Table I and the Fayet-Iliopoulos terms $\xi_1 = \xi_N \equiv \xi$ described above, and to bundle all of the remaining complexities in terms of a single kinetic-mixing parameter χ.

Not all values of the parameter χ lead to self-consistent theories, however; we must also ensure that the kinetic-mixing matrix X_{ab} in Eq. (3) is invertible with positive (real) eigenvalues. For $N = 2$, we find that this requires $|\chi| < 1$, while for $N = 3$, 4, and 5 this requires $|\chi| < 1/\sqrt{2}$, $|\chi| < 2/(1+\sqrt{5})$, and $|\chi| < 1/\sqrt{3}$ respectively. The behavior of the maximum allowed value of $|\chi|$ as a function of N is shown in Fig. 1.

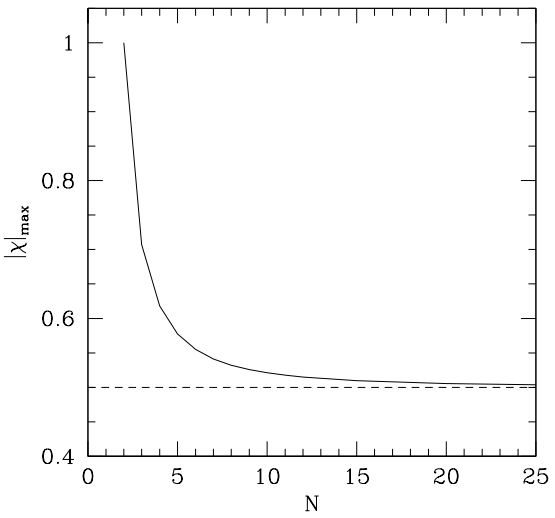

FIG. 1: The maximum allowed value of $|\chi|$, plotted as a function of N. As $N \to \infty$, we see that $|\chi|_{\rm max}$ asymptotically approaches 1/2 from above.

For arbitrary N, we see from Fig. 1 that the maximum allowed value of $|\chi|$ always exceeds 1/2, and asymptotically approaches 1/2 as $N \to \infty$. Moreover, we find that negative values of χ do not lead to the metastable vacuum towers which are our main interest in this paper. As a result, we shall simplify matters by restricting our attention to the range

$$0 \ < \ \chi \ < \ 1/2 \ . \quad (5)$$

(Indeed, only in Sect. V shall we consider the $\chi = 1/2$ limit.) Likewise, our orbifold moose structure for any length N possesses a reflection symmetry under which the combined transformations $\xi_a \to -\xi_{N+1-a}$, $g_a \to g_{N+1-a}$, $\xi_2 \to -\xi_2$, and $\Phi_j \to \Phi_{N-j+2}$ leaves the physics invariant. This means that the scalar potential in a theory of given N with $\xi < 0$ will be identical to that with $\xi > 0$, save that the role played by Φ_1 in the former is played by Φ_{N+1} in the latter, and so forth. As a result, we will restrict our attention to situations with

$$\xi \ > \ 0 \ . \quad (6)$$

Finally, our model also has a reflection symmetry under $\lambda \to -\lambda$, as a result of which we can further restrict to $\lambda > 0$. However, for each N, we shall find that there is actually a minimum positive value λ_N^* which is needed in order for our entire tower of $N-1$ vacua to be (meta)stable. The derivation and interpretation of this

critical value λ_N^* will be discussed further below. We shall therefore actually restrict to the range

$$\lambda \ > \ \lambda_N^* \tag{7}$$

in much of what follows.

Thus, to summarize, our models are defined in terms of N different $U(1)_a$ gauge groups and $N+1$ different chiral superfields Φ_i, with charges indicated in Table I. This structure can be indicated pictorially through the moose diagram in Fig. 2, which shows not only the $U(1)_a$ gauge groups but also the Φ_i fields which provide nearest-neighbor "links" between them as well as the χ parameter which governs their universal nearest-neighbor kinetic mixing. For each value of $N \geq 2$, our models are therefore governed by four continuous parameters, namely g, χ, ξ, and λ, subject to the bounds in Eqs. (5), (6) and (7). Note that a similar model, but with $\chi = 0$, was considered in Ref. [13].

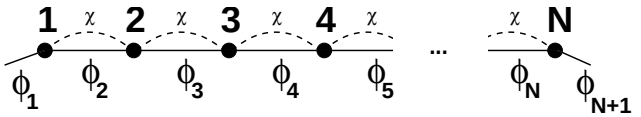

FIG. 2: The "moose" diagram for our series of models. The N sites [each representing a $U(1)$ gauge group] are connected by links corresponding to the chiral superfields Φ_i, and experience nearest-neighbor kinetic mixing governed by a universal parameter χ.

Our main interest in this paper is in the vacuum structure of these models. This in turn is governed by their corresponding scalar potentials. In general, the scalar potential for such a supersymmetric gauge theory coupled to matter includes both D-term and F-term contributions and can be written in the form

$$V \ = \ \tfrac{1}{2}\sum_{a=1}^{N} g^2 \hat{D}_a^2 + \sum_{i=1}^{N+1} |F_i|^2 \ , \tag{8}$$

where each gauge-group factor has a common coupling g and where

$$\hat{D}_a = \hat{\xi}_a + \sum_{i=1}^{N+1} \hat{Q}_{ai} |\phi_i|^2 \ , \qquad F_i = -\frac{\partial W^*}{\partial \phi_i^*} \ . \tag{9}$$

For any choice of parameters $\{g, N, \chi, \xi, \lambda\}$, the extrema of the scalar potential can then be obtained by solving the $N+1$ coupled simultaneous equations

$$\frac{\partial V}{\partial \phi_i} = 0 \qquad (i = 1, \ldots, N+1) \ . \tag{10}$$

However, a solution is a local minimum only if the eigenvalues of the $2(N+1) \times 2(N+1)$ mass matrix

$$\mathcal{M}^2 \ \equiv \ \begin{pmatrix} \frac{\partial^2 V}{\partial \phi_i^* \partial \phi_j} & \frac{\partial^2 V}{\partial \phi_i^* \partial \phi_j^*} \\ \frac{\partial^2 V}{\partial \phi_i \partial \phi_j} & \frac{\partial^2 V}{\partial \phi_i \partial \phi_j^*} \end{pmatrix} \tag{11}$$

are all non-negative and the number of zero eigenvalues is precisely equal to the number of Goldstone bosons eaten by the massive gauge fields. (Indeed, additional zeroes would indicate the presence of classical flat directions.) In what follows, however, we will use the term "vacuum" loosely to refer to any extremum of the potential and employ adjectives such as "stable" and "unstable" to distinguish the eigenvalues of the mass matrix. Of course, a "metastable" vacuum exists only when two or more vacua exist and are stable according to the above definitions; all but the vacuum with lowest energy are considered metastable.

Note that the scalar potential V will in general be a function of only the absolute squares of fields. As a result, we can take all non-zero vacuum expectation values $v_i \equiv \langle \phi_i \rangle$ to be real and positive without loss of generality.

Also note that while the F-terms are insensitive to the kinetic mixing, the D-terms in Eq. (9) are calculated in terms of the charges $\hat{Q}_{ai}$ and Fayet-Iliopoulos coefficients $\hat{\xi}_a$ in the *orthonormalized* basis given in Eq. (4). It is apparent from the form of Eq. (8) that while $\hat{D}_a$ depends on the choice of $\mathcal{O}$ within the matrix M, the scalar potential as a whole is insensitive to this choice. By contrast, the rescaling matrix $\mathcal{S}$ within M is physical, modifying the D-terms in a non-trivial way. It is in this manner that the effects of kinetic mixing are felt in the vacuum structure of the theory.

Finally, we emphasize that we shall deem an extremum of the scalar potential V to be (meta)stable only if there are neither flat directions nor negative eigenvalues in the mass matrix. These two restrictions are rather severe, since most models tend to give extrema which have either tachyonic modes or flat directions.

In the rest of this paper, we shall simplify our analysis by scaling out the gauge coupling g in the manner discussed in Ref. [14]. Specifically, we shall define the rescaled quantities $\xi' \equiv g\xi$, $\lambda' \equiv \lambda/g^{N/2}$, and $\Phi_i' \equiv \sqrt{g}\Phi_i$, holding all other quantities fixed. We shall then eliminate explicit dependence on ξ' by further rescaling all dimensionful quantities by appropriate powers of ξ' in order to render them dimensionless. Specifically, we shall define $\lambda'' \equiv \lambda'/(\xi')^{1-N/2}$, $\Phi_i'' \equiv \Phi_i'/\sqrt{\xi'}$, and $V'' \equiv V/(\xi')^2$. In practical terms, the net effect of these two rescalings is that we simply rewrite all of our original expressions in terms of the new variables $\lambda'' \equiv \xi^{N/2-1}\lambda/g$, $V'' \equiv V/(g\xi)^2$, and $\Phi_i'' \equiv \Phi_i/\sqrt{\xi}$, and then drop the double primes. Thus, for each $N \geq 2$, our models can be analyzed purely in terms of a single kinetic-mixing parameter χ and the rescaled (dimensionless) Wilson-line coefficient λ defined above; the resulting vacuum energies V and field VEV's $v_i \equiv \langle \Phi_i \rangle$ will then be dimensionless as well. Finally, we shall adopt a notation (first introduced in Ref. [13]) wherein we describe a particular field configuration of VEV's v_i as belonging to a class denoted $\{\mathbf{p}, \mathbf{q}, ...\}$ if the only non-zero VEV's for the vacuum solutions in this class are v_p, v_q, and so forth. For example, $\{\mathbf{1}, \mathbf{2}, \mathbf{4}\}$ will refer to a vacuum configuration in which v_1, v_2, and v_4 are non-zero, with all other VEV's vanishing.

Our claim, then, is that for each N, our model gives rise to a tower consisting of $N-1$ vacuum solutions. Specifically, for each N, we claim that the corresponding model will give rise to a true stable ground state along with a series of $N-2$ metastable ground states with higher and higher vacuum energies.

A. Example: $N = 3$

We shall begin the analysis of our models by focusing on a simple example: the $N = 3$ special case, which consists of three $U(1)$ gauge groups and four chiral superfields. The scalar potential in this case is given by $V = V_D + V_F$, where

$$\begin{aligned} V_D &= \frac{1}{4}\left(|\phi_1|^2 - |\phi_2|^2 - |\phi_3|^2 + |\phi_4|^2\right)^2 \\ &\quad + \frac{1}{8(1-\sqrt{2}\chi)}\Big[2 - |\phi_1|^2 - (\sqrt{2}-1)|\phi_2|^2 \\ &\qquad + (\sqrt{2}-1)|\phi_2|^2 + |\phi_4|^2\Big]^2 \\ &\quad + \frac{1}{8(1+\sqrt{2}\chi)}\Big[2 - |\phi_1|^2 + (\sqrt{2}+1)|\phi_2|^2 \\ &\qquad - (\sqrt{2}+1)|\phi_2|^2 + |\phi_4|^2\Big]^2 , \end{aligned} \tag{12}$$

and

$$V_F = |\lambda|^2 \sum_{i=1}^{4} \frac{|\phi_1|^2|\phi_2|^2|\phi_3|^2|\phi_4|^2}{|\phi_i|^2} . \tag{13}$$

In these expressions, of course, ϕ_i denotes the (complex) scalar component of the chiral supermultiplet Φ_i.

Given the scalar potential, it is then a straightforward matter to calculate the vacuum structure of this potential. Our results are as follows. Defining

$$\lambda_3^* \equiv \frac{1}{\sqrt{\chi(1+\chi)}} , \tag{14}$$

we find that there are two (meta)stable vacua in this model for all $\lambda > \lambda_3^*$. The first vacuum state (which we shall call the $n = 1$ vacuum) has energy $V_1 = 1/2$ and corresponds to the solution with

$$n = 1 : \qquad v_1^2 = 1+\chi , \qquad v_2^2 = \chi , \qquad v_3^2 = v_4^2 = 0 . \tag{15}$$

By contrast, the second vacuum state (which we shall call the $n = 2$ vacuum) has vacuum energy $V_2 = \frac{1}{4}(1-\chi)^{-1}$ and corresponds to the solution with

$$n = 2 : \qquad v_1^2 = \frac{2-\chi}{2-2\chi} , \qquad v_3^2 = \tfrac{1}{2} , \qquad v_2^2 = v_4^2 = 0 . \tag{16}$$

We thus see that the $n = 1$ vacuum is of $\{\mathbf{12}\}$-type, while the $n = 2$ vacuum is of $\{\mathbf{13}\}$-type. As emphasized above, both of these solutions are *stable* (without any flat or tachyonic directions) for all $\lambda > \lambda_3^*$; however, since $V_1 > V_2$ for all $\chi < 1/2$, we see that the $n = 2$ vacuum is the true ground state in this theory, while the $n = 1$ vacuum is only metastable. This vacuum configuration is sketched in Fig. 3.

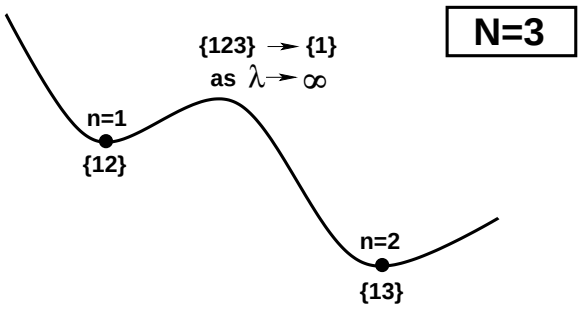

FIG. 3: A sketch of the vacuum structure of the $N = 3$ model. For $\lambda > \lambda_3^*$, the corresponding scalar potential gives rise to two distinct minima: a $\{\mathbf{13}\}$ vacuum which serves as the true ground state of the theory, and a $\{\mathbf{12}\}$ vacuum which serves as an additional, metastable vacuum. These two minima are separated by a saddle-point $\{\mathbf{123}\}$ extremum which reduces to the $\{\mathbf{1}\}$ extremum in the formal $\lambda \to \infty$ limit. Note that this sketch is actually a two-dimensional representation of potential energy contours in a three-dimensional field space parametrized by $\{v_1^2, v_2^2, v_3^2\}$.

Note that for $\lambda > \lambda_3^*$, the $n = 1$ and $n = 2$ vacua are separated by a potential barrier whose lowest point is a $\{\mathbf{123}\}$ saddle-point extremum of the scalar potential. Unlike the field-space solutions for the $n = 1$ and $n = 2$ vacua, which are λ-independent, the field-space solution for this saddle point depends quite strongly on λ. This is shown in Fig. 4, where the explicit solutions for $\{v_1^2, v_2^2, v_3^2\}$ are plotted for $\lambda > \lambda_3^*$.

It will be useful to understand how this vacuum structure deforms as a function of λ. Naïvely, one might suspect that taking $\lambda \to \infty$ would cause the height of this saddle-point barrier to diverge. However, we see from Fig. 4 that this is not the case: the scalar potential V and all of the field VEV's v_i^2 quickly reach finite asymptotes. Indeed, in the formal $\lambda \to \infty$ limit, we see that $v_2^2, v_3^2 \to 0$, whereupon our $\{\mathbf{123}\}$ saddle-point solution reduces to the $\{\mathbf{1}\}$ solution given by

$$v_1^2 = \frac{1}{1-\chi^2} , \qquad v_2^2 = v_3^2 = v_4^2 = 0 \tag{17}$$

with $V_{12} = \frac{1}{2}(1-\chi^2)^{-1}$.

The above results are valid for all $\lambda > \lambda_3^*$. However, it will also be important for us to understand what happens as we reduce the value of λ below λ_3^*. Since λ sets the scale for the barrier height between the two vacua in Fig. 3, reducing λ has the effect of reducing the barrier height between the two vacua. This in turn will destabilize our metastable vacuum. Specifically, we see from Fig. 4 that $\lambda_3^* \equiv 1/\sqrt{\chi(1+\chi)}$ is nothing but the critical value of λ at which the barrier height becomes

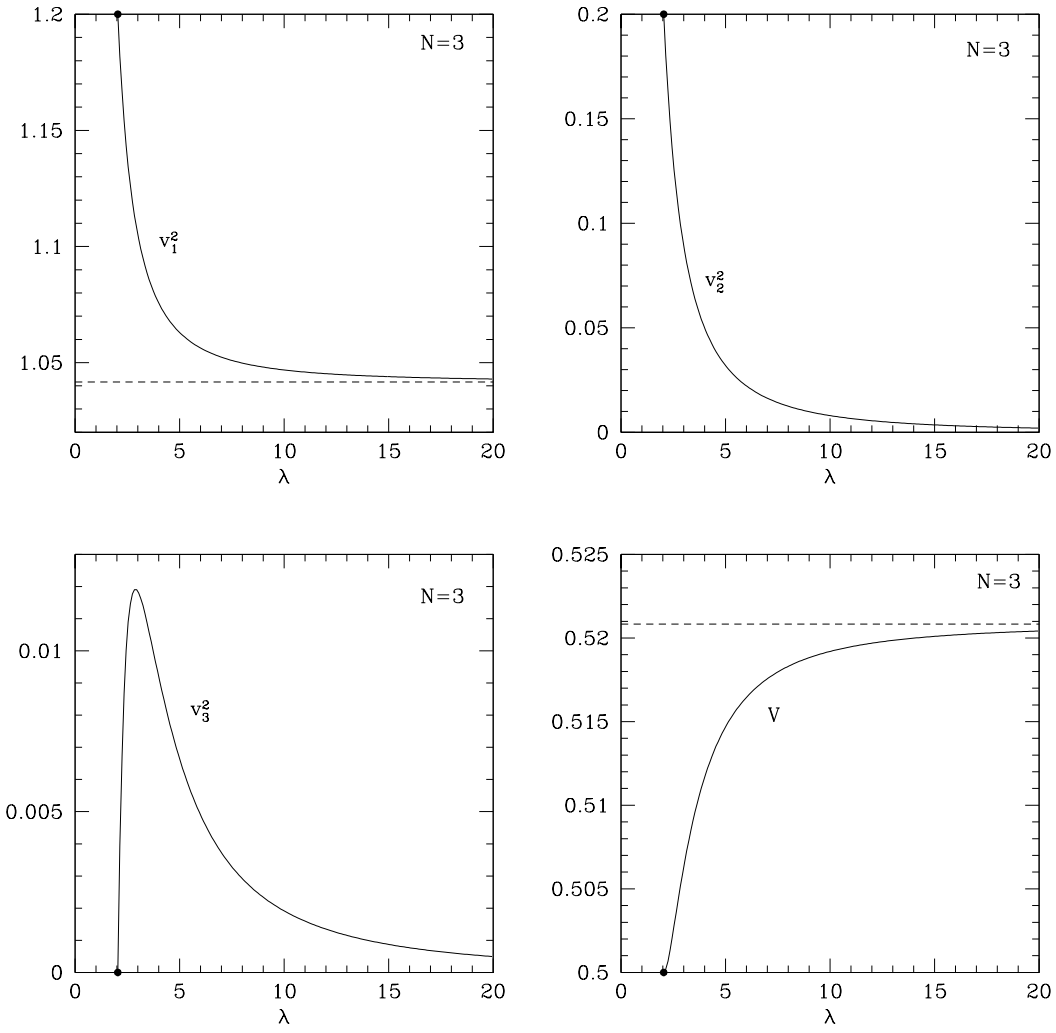

FIG. 4: The $\{\mathbf{123}\}$ saddle-point solution for $N = 3$ and $\chi = 1/5$, plotted as a function of $\lambda \geq \lambda_3^* = 5/\sqrt{6} \approx 2.04$. Here we show the non-zero field VEV's $|v_1|^2$ (upper left plot), $|v_2|^2$ (upper right plot), and $|v_3|^2$ (lower left plot), as well as the corresponding scalar potential V (lower right plot). While each of these quantities varies with λ, they quickly reach formal asymptotes as $\lambda \to \infty$.

equal to V_1. At this critical value, the $\{\mathbf{123}\}$ saddle-point solution shown in Fig. 4 actually merges with the metastable $n = 1$ vacuum solution (which is of $\{\mathbf{12}\}$-type) and thereby destabilizes it. Thus, as we take λ below λ_3^*, we lose the $n = 1$ vacuum. In order to emphasize that this is the critical λ-value at which the $n = 1$ vacuum is destabilized, we shall also refer to λ_3^* as $\lambda_{3,1}^*$.

Taking λ still lower, we ultimately reach a second critical value $\lambda_{3,2}^* \equiv \sqrt{2/(2-\chi)}$ at which even the $n = 2$ vacuum becomes destabilized. In this case, a new $\{\mathbf{123}\}$ solution becomes stable and serves as the ground state of the theory for all $\lambda < \lambda_{3,2}^*$.

These two critical values of λ for the $N = 3$ case are plotted in Fig. 5 as a function of the kinetic-mixing parameter χ. Note, in particular, that $\lambda_{3,1}^*$ diverges as $\chi \to 0$. This shows that the stability of the $n = 1$ metastable vacuum solution relies not only on having a sufficiently large value of λ, but also on the existence of non-zero kinetic mixing. Note also that

$$0 \;<\; \lambda_{3,2}^* \;<\; \lambda_{3,1}^* \qquad \text{for all } \; 0 < \chi < 1/2 \; . \tag{18}$$

This indicates that as reduce λ below $\lambda_3^* = \lambda_{3,1}^*$, our $N = 3$ metastable "tower" destabilizes from the top down, with the $n = 1$ metastable vacuum destabilizing before the $n = 2$ vacuum. It is for this reason that we can associate λ_3^* (the critical λ-value for stability for the entire tower) with $\lambda_{3,1}^*$ (the critical λ-value for stability of the highest vacuum).

We see, then, that our $N = 3$ model gives rise to two vacuum solutions (one stable ground state and one metastable state above it) for all $\lambda > \lambda_3^* = \lambda_{3,1}^*$. The solutions for these vacua are λ-independent, and depend

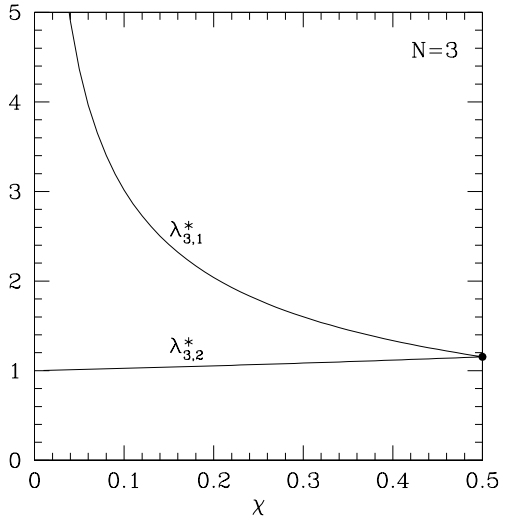

FIG. 5: Critical λ-values for the $N = 3$ model, plotted as functions of χ. Here $\lambda^*_3 = \lambda^*_{3,1} = 1/\sqrt{\chi(\chi+1)}$ and $\lambda^*_{3,2} = \sqrt{2/(2-\chi)}$. For $\lambda > \lambda^*_{3,1}$, both the $n = 1$ and $n = 2$ vacua are stable, while for $\lambda^*_{3,2} < \lambda \leq \lambda^*_{3,1}$, the $n = 1$ vacuum is destabilized and only the $n = 2$ vacuum is stable. For $\lambda \leq \lambda^*_{3,2}$, even the $n = 2$ vacuum is destabilized; in this range a new $\{\mathbf{123}\}$ solution becomes stable and serves as the ground state of the theory.

only on χ. However, the barrier height between these two vacua (and hence the stability of the metastable vacuum) depends intimately on both χ and λ, and formally reaches an asymptote as $\lambda \to \infty$.

B. Example: $N = 4$

Having discussed the vacuum structure of the $N = 3$ model, we now turn to the $N = 4$ model. In this case, there are four $U(1)$ gauge groups and five chiral superfields. Defining

$$\lambda^*_4 \equiv \frac{1}{\chi\sqrt{1+\chi}} , \tag{19}$$

we find that the vacuum structure now consists of *three* vacuum solutions, each without tachyonic or flat directions, for all $\lambda > \lambda^*_4$. The $n = 1$ vacuum has energy $V_1 = 1/2$, just as in the $N = 3$ case, and corresponds to the solution with

$$n = 1 : \quad \begin{cases} v_1^2 = 1+\chi , \quad v_2^2 = v_3^2 = \chi , \\ v_4^2 = v_5^2 = 0 , \end{cases} \tag{20}$$

while the $n = 2$ vacuum has energy $V = \frac{1}{4}(1-\chi)^{-1}$, again just as in the $N = 3$ case, and now corresponds to the solution with

$$n = 2 : \quad \begin{cases} v_1^2 = \frac{2-\chi}{2-2\chi} , \quad v_2^2 = \frac{\chi}{2-2\chi} , \\ v_4^2 = \frac{1}{2} , \quad v_3^2 = v_5^2 = 0 . \end{cases} \tag{21}$$

The solutions in Eqs. (20) and (21) are clearly the $N = 4$ generalizations of the corresponding $N = 3$ solutions in Eqs. (15) and (16) respectively. However, the crucial new feature for the $N = 4$ case is the appearance of an additional vacuum state of even lower energy. This vacuum state, which we shall refer to as the $n = 3$ vacuum, has energy $V_3 = \frac{1}{2}(3-4\chi)^{-1}$ and corresponds to the solution with

$$n = 3 : \quad \begin{cases} v_1^2 = \frac{3(1-\chi)}{3-4\chi} , \quad v_3^2 = \frac{1-\chi}{3-4\chi} , \\ v_4^2 = \frac{2-3\chi}{3-4\chi} , \quad v_2^2 = v_5^2 = 0 . \end{cases} \tag{22}$$

This vacuum structure is sketched in Fig. 6. Note that just as in the $N = 3$ case, these vacuum solutions are all λ-independent.

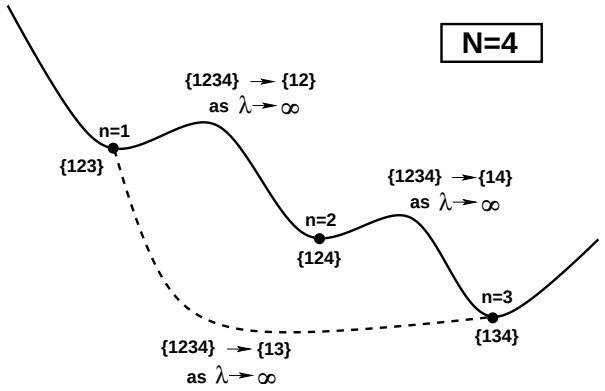

FIG. 6: A sketch of the vacuum structure of the $N = 4$ model. For $\lambda > \lambda^*_4$, the corresponding scalar potential gives rise to three distinct minima: a $\{\mathbf{134}\}$ vacuum which serves as the true ground state of the theory, and two additional metastable vacua of types $\{\mathbf{123}\}$ and $\{\mathbf{124}\}$ above it. These three vacua are separated by three different saddle-point extrema which are each different solutions of $\{\mathbf{1234}\}$-type; in the formal $\lambda \to \infty$ limit, these reduce to the different two-VEV solutions shown. Note that this sketch is actually a two-dimensional representation of potential energy contours in a four-dimensional field space parametrized by $\{v_1^2, v_2^2, v_3^2, v_4^2\}$.

For $\lambda > \lambda^*_4$, the $n = 1$, $n = 2$, and $n = 3$ vacua are separated by potential barriers whose lowest points are all $\{\mathbf{1234}\}$ saddle-point extrema of the scalar potential. Unlike the field-space solutions for the (meta)stable vacua, the field-space solutions for these saddle points depend quite strongly on λ. However, in the formal $\lambda \to \infty$ limit, these solutions all quickly reach finite asymptotes. For example, the asymptotic saddle-point solution between the $n = 1$ and $n = 2$ vacua is of $\{\mathbf{12}\}$-type and is given by

$$(1,2) : \quad \begin{cases} v_1^2 = \frac{1}{1-\chi^2} , \quad v_2^2 = \frac{\chi^2}{1-\chi^2} , \\ v_3^2 = v_4^2 = v_5^2 = 0 \end{cases} \tag{23}$$

with energy $V_{12} = \frac{1}{2}(1-\chi^2)^{-1}$. This is the $N = 4$ analogue of the $N = 3$ asymptotic saddle-point solution in

Eq. (17), and continues to have the same energy V_{12}. However, in the $N = 4$ case there are also additional saddle-point solutions which involve the new $n = 3$ vacuum. Specifically, the asymptotic saddle-point solution which lies directly between the $n = 1$ and $n = 3$ vacua is of $\{\mathbf{13}\}$-type and is given by

$$(1,3): \quad \begin{cases} v_1^2 = \frac{2(1-\chi)}{2-2\chi-\chi^2} \ , \quad v_3^2 = \frac{\chi(1-\chi)}{2-2\chi-\chi^2} \ , \\ v_2^2 = v_4^2 = v_5^2 = 0 \end{cases} \tag{24}$$

with energy $V_{13} = (1-\chi)/(2-2\chi-\chi^2)$, while the asymptotic saddle-point solution between the $n = 2$ and $n = 3$ vacua is of $\{\mathbf{14}\}$-type and is given by

$$(2,3): \quad \begin{cases} v_1^2 = \frac{2(1-\chi)}{2-2\chi-\chi^2} \ , \quad v_4^2 = \frac{1-\chi-\chi^2}{2-2\chi-\chi^2} \ , \\ v_2^2 = v_3^2 = v_5^2 = 0 \end{cases} \tag{25}$$

with energy $V_{23} = \frac{1}{2}(2-2\chi-\chi^2)^{-1}$.

This vacuum structure emerges for all $\lambda > \lambda_4^*$. However, just as in the $N = 3$ case, we find that reducing λ below λ_4^* tends to destabilize our vacuum tower. Specifically, one finds that there are now *three* critical λ-values, denoted $\lambda_{4,1}^*$, $\lambda_{4,2}^*$, and $\lambda_{4,3}^*$, at which the $n = 1$, $n = 2$, and $n = 3$ vacua are respectively destabilized. These three critical values are given by

$$\begin{aligned} \lambda_{4,1}^* &\equiv \frac{1}{\chi\sqrt{1+\chi}} \\ \lambda_{4,2}^* &\equiv 2\sqrt{\frac{(1-\chi)}{\chi(2-\chi)}} \\ \lambda_{4,3}^* &\equiv \frac{3-4\chi}{1-\chi}\sqrt{\frac{1}{3(2-3\chi)}} \ , \end{aligned} \tag{26}$$

and all three are plotted in Fig. 7 as functions of χ. We see from this figure that

$$0 \ < \ \lambda_{4,3}^* \ < \ \lambda_{4,2}^* \ < \ \lambda_{4,1}^* \tag{27}$$

for all $0 < \chi < 1/2$. This implies that just as in the $N = 3$ case, our vacuum tower destabilizes from the top down as we reduce λ below $\lambda_{4,1}^*$. As a result of Eq. (27), we see that λ_4^* (*i.e.*, the critical λ-value for stabilizing the entire $N = 4$ vacuum tower) is nothing but $\lambda_{4,1}^*$ (the maximum of the individual values $\lambda_{4,n}^*$ for stabilizing any of the individual vacua in the tower). It is this observation which underlies the identification given in Eq. (19). We also observe from Fig. 7 that non-zero kinetic mixing is also required in order for the stability of our metastable vacua.

It is clear that the $N = 4$ case is a direct generalization of the $N = 3$ case. Once again, the vacuum solutions are λ-independent, while the barrier heights (and hence the stability of these vacuum solutions) are λ-dependent. Moreover, the energies associated with the $n = 1$ and $n = 2$ vacua, as well as the barrier between them, are unchanged in passing from the $N = 3$ case to the $N = 4$ case. Indeed, the primary new feature in passing from the $N = 3$ case to the $N = 4$ case is the emergence of a new vacuum solution, our so-called $n = 3$ vacuum, which "slides in" *below* the previous bottom of the tower and becomes the new ground state of the theory for all $\lambda > \lambda_{4,3}^*$. As a result, our previous $n = 2$ ground state in the $N = 3$ theory now becomes the first-excited metastable state in the $N = 4$ theory, and our tower of metastable vacua has grown by one additional metastable vacuum. We stress again that all of these vacua are either strictly stable or strictly metastable. In particular, they contain neither tachyonic masses nor flat directions.

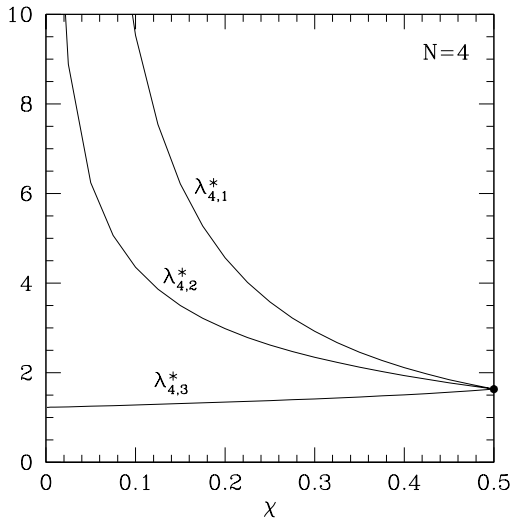

FIG. 7: Critical λ-values for the $N = 4$ model, plotted as functions of χ. For $\lambda > \lambda_4^* = \lambda_{4,1}^*$, all three of our vacua are stable, while for $\lambda_{4,2}^* < \lambda \leq \lambda_{4,1}^*$, the $n = 1$ vacuum is destabilized and for $\lambda_{4,3}^* < \lambda \leq \lambda_{4,2}^*$, both the $n = 1$ and $n = 2$ vacua are destabilized. Finally, for $\lambda \leq \lambda_{4,3}^*$, even the $n = 1$ vacuum is destabilized; in this range a new $\{\mathbf{1234}\}$ solution becomes stable and serves as the ground state of the theory.

C. Results for general N

We now turn to the case with general N. As might be expected, the pattern we have seen in passing from the $N = 3$ case to the $N = 4$ case continues without major alteration. For general N and for λ exceeding a critical value λ_N^*, we find that our model has a vacuum structure consisting of a tower of $N-1$ stable vacua: a single stable ground state, and $N-2$ metastable vacua above it. As in the $N = 3$ and $N = 4$ cases discussed above, we shall number these vacua from the top down with an index n, so that the $n = 1$ vacuum sits at the top of the tower and the $n = N-1$ vacuum (the true ground state of the theory) sits at the bottom.

We then find that the n-vacuum has energy

$$V_n \;=\; \tfrac{1}{2}\left(\frac{1}{\chi R_n}\right)\;, \qquad 1\le n\le N-1 \tag{28}$$

where

$$R_n \;\equiv\; \left(\frac{1}{\chi}-2\right)n+2\;, \tag{29}$$

and corresponds to the solution with

$$v_j^2 = \begin{cases} 1+1/R_n & \text{for } j=1 \\ 1/R_n & \text{for } 2\le j\le N-n \\ 0 & \text{for } j=N-n+1 \\ (R_{j-N+n-1}-1)/R_n & \text{for } N-n+2\le j\le N \\ 0 & \text{for } j=N+1\;. \end{cases} \tag{30}$$

As evident from these VEV's, this is clearly a solution of $\{\mathbf{1},...,\mathbf{N-n},\mathbf{N-n+2},...,\mathbf{N}\}$-type. It is easy to verify that these results reduce to those already quoted for the $N=3$ and $N=4$ special cases. Note that the vacuum energies V_n along the tower are independent of N, as expected; indeed, all that depends on N are the number of such vacua and their precise field VEV's. Also note that $V_{N-1}\to 0$ as $N\to\infty$.

As in the previous special cases with $N=3$ and $N=4$, any two vacua n and n' are separated by a saddle-point solution. In the formal $\lambda\to\infty$ limit, we find that this barrier height asymptotes to the value

$$V_{nn'} \;=\; \frac{1}{2\chi}\left(\frac{R_{n'-n}}{R_n R_{n'-n}-1}\right) \tag{31}$$

where R_n is defined in Eq. (29) and where we have taken $n'>n$. Note that $V_{nn'}$ is also independent of N. The corresponding asymptotic saddle-point solutions are given by

$$v_j^2 = \begin{cases} \frac{R_n R_{n'-n}}{R_n R_{n'-n}-1} & \text{for } j=1 \\ \frac{1}{R_n R_{n'-n}-1} & \text{for } 2\le j\le N-n' \\ 0 & \text{for } j=N-n'+1 \\ \frac{R_{j-N+n'-1}-1}{R_n R_{n'-n}-1} & \text{for } N-n'+2\le j\le N-n \\ 0 & \text{for } j=N-n+1 \\ \frac{R_{n'-n}(R_{j-N+n-1}-1)-1}{R_n R_{n'-n}-1} & \text{for } N-n+2\le j\le N \\ 0 & \text{for } j=N+1\;. \end{cases} \tag{32}$$

These results are plotted in Fig. 8 for the $N=20$ model. Clearly, the vacuum structure of this model consists of a ground-state vacuum along with a tower of 18 metastable vacua above it. In Fig. 8, we have shown the vacuum energies of these vacua, along with the asymptotic energies of the saddle-point barriers which connect

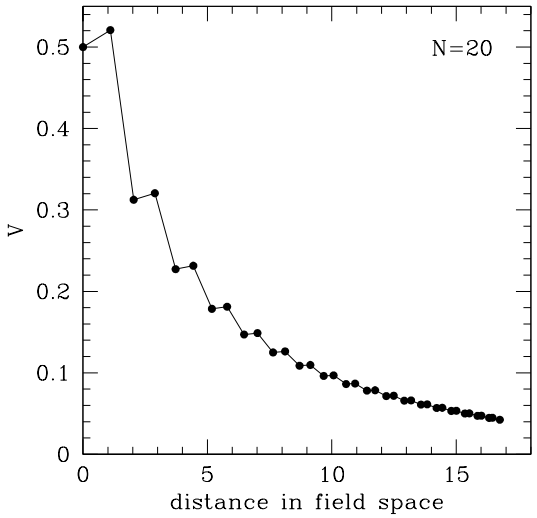

FIG. 8: The vacuum structure of the $N=20$ model, plotted for $\chi=1/5$. Each of the local minimum points corresponds to a (meta)stable vacuum state, while each local maximum point corresponds to the saddle-point configuration which directly connects the nearest-neighbor vacuum configurations on either side. For the purposes of this plot, we have then simply connected these points sequentially with straight lines. The vertical axis indicates the energies of these vacua or saddle points (the latter in their asymptotic limits), while the horizontal axis indicates the cumulative distances in field space along a trajectory which begins at the $n=1$ vacuum and then proceeds along straight-line path segments to the $(1,2)$ saddle point, then to the $n=2$ vacuum, then to the $(2,3)$ saddle point, and so forth.

"nearest-neighbor" vacua, as functions of a cumulative distance in field space along a path that winds through each vacuum configuration and over each saddle point as it comes down the tower, vacuum by vacuum. In essence, then, this figure forms a linear "picture" of the tower.

Despite the relative simplicity of Fig. 8, it is worth emphasizing that the geometry of the metastable vacuum tower in the full $(N+1)$-dimensional field space is rather non-trivial. For example, although the vacuum and saddle-point energies are plotted in Fig. 8 versus a cumulative, integrated distance as we wind our way down the vacuum tower, we could have just as easily defined the field-space distance associated with any vacuum or saddle point in terms of its straight-line distance directly back to a reference vacuum (such as the $n=1$ vacuum at the top of the tower). The difference between these two different notions of distance is shown in Fig. 9 for the $N=20$ case. Indeed, as evident from the actual solutions given Eq. (30), the vacua in our vacuum tower actually lie along a "spiral" or "helix" in the N-dimensional $v_{N+1}=0$ subspace of our full $(N+1)$-dimensional field space.

It is also important to emphasize that Fig. 8 shows only

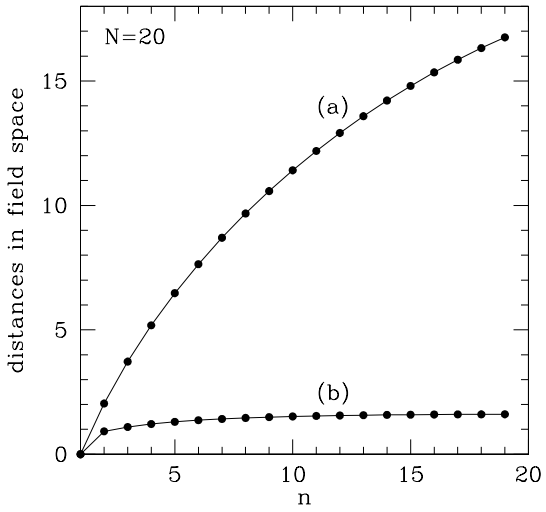

FIG. 9: The geometry of our metastable vacuum towers in field space, here illustrated for the $N = 20$ model with $\chi = 1/5$. For each n-vacuum ($n = 1, ..., 19$) in the $N = 20$ vacuum tower, we have plotted two different notions of corresponding field-space distance. In curve (a), we have plotted the cumulative distance (as used in Fig. 8) that accrues as we wind our way from the top of the tower down to the n-vacuum, passing through nearest-neighbor saddle points along the way. By contrast, in curve (b), we have plotted the direct straight-line distance between each n-vacuum and the reference $n = 1$ vacuum at the top of the tower. The dramatic difference between these two curves is a reflection of the fact the vacua in our vacuum tower actually lie along a "spiral" or "helix" in the full 20-dimensional field space.

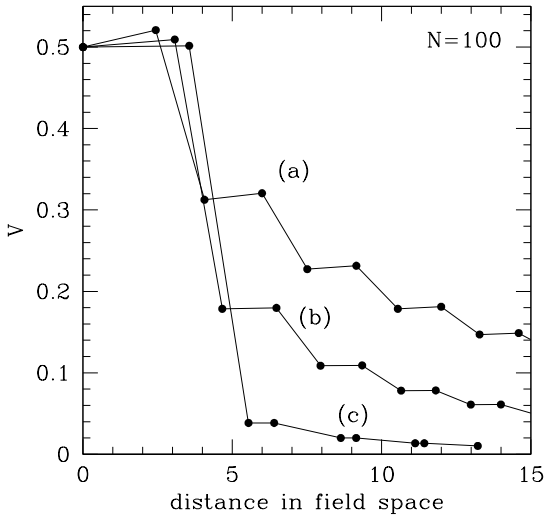

FIG. 10: The upper portions of the $N = 100$ vacuum tower with $\chi = 1/5$, plotted for saddle-point "hops" of fixed magnitudes (a) $\Delta n = 1$, (b) $\Delta n = 3$, and (c) $\Delta n = 20$ respectively. Note that the energy of a given vacuum is independent of how it is reached; for example, we see that the $n = 4$ vacuum has the same energy whether it is realized as the fourth minimum on the $\Delta n = 1$ curve or the second minimum on the $\Delta n = 3$ curve. However, the corresponding field-space distances relative to the top of the tower are generally smaller when larger hops are utilized when descending.

those saddle-point barriers which exist between nearest-neighbor vacua along the vacuum tower. In actuality, however, there are saddle-point barriers which exist directly between any two vacua (n, n'). As a result, it is possible to imagine descending through the vacuum tower taking "hops" with different values of Δn at each step. Fig. 10 provides an illustration of the effects of different possiblities.

Finally, we turn to the one remaining issue: the critical value $\lambda^*_{N,n}$ at which the $n^{\rm th}$ vacuum in the tower is destabilized. In general, for any $N \geq 2$ and $1 \leq n \leq N-1$, it turns out that $\lambda^*_{N,n}$ is given by

$$\lambda^{*2}_{N,n} \;=\; y^n \,\frac{\Gamma(y)}{\Gamma(n+y)}\,\frac{R_n^{N-2}}{\chi(1+R_n)} \tag{33}$$

where $y \equiv \chi/(1-2\chi) = n/(R_n - 2)$ and where $\Gamma(z)$ is the Euler Γ-function [for which $\Gamma(z) = (z-1)!$ when $z \in \mathbb{Z}^+$]. It is straightforward to verify that these expressions reduce to the corresponding expressions for the $N = 3$ and $N = 4$ cases plotted in Figs. 5 and 7 respectively. For example, using the result in Eq. (33), we find that

$$\lambda^*_{N,1} \;\equiv\; \sqrt{\frac{1}{1+\chi}}\;\chi^{1-N/2}\;. \tag{34}$$

In Fig. 11, we plot the values of $\lambda^*_{N,n}$ as functions of χ for $N = 20$ and $1 \leq n \leq 19$. Unlike the simpler $N = 3$ and $N = 4$ cases, however, we see that it is no longer true that $\lambda^*_{N,n} > \lambda^*_{N,n'}$ for any $n < n'$. Instead, as N increases, we see that a complicated "crossing" pattern develops as a function of χ. As a result of this crossing pattern, the value of n which results in the maximum value of $\lambda^*_{N,n}$ itself varies with χ, as shown in Fig. 12. Nevertheless, for any value of χ, we see that our entire vacuum tower will be stable if $\lambda > \lambda^*_N$, where

$$\lambda^*_N \;\equiv\; \max_{1\leq n\leq N-1} \lambda^*_{N,n}\;. \tag{35}$$

Thus, λ^*_N corresponds to the upper "envelope" of the curves shown in Fig. 11.

The crossing pattern shown in Fig. 11 implies that our tower of metastable vacua will experience a non-trivial destabilization pattern as λ is reduced from infinity. For any value of χ in the range $0 < \chi < 1/2$, the first vacuum to be destabilized is indicated in Fig. 12. This serves as the initial destabilization point on the tower. Reducing λ still further then induces a destabilization of the vacua immediately above and below this point, and further reductions in λ result in a destabilization "wave" which simultaneously runs both up and down the vacuum tower from this initial point until ultimately all vacua are destabilized.

Finally, the dependence of λ^*_N on N is shown in Fig. 13. We see that λ^*_N generally grows rather quickly with N.

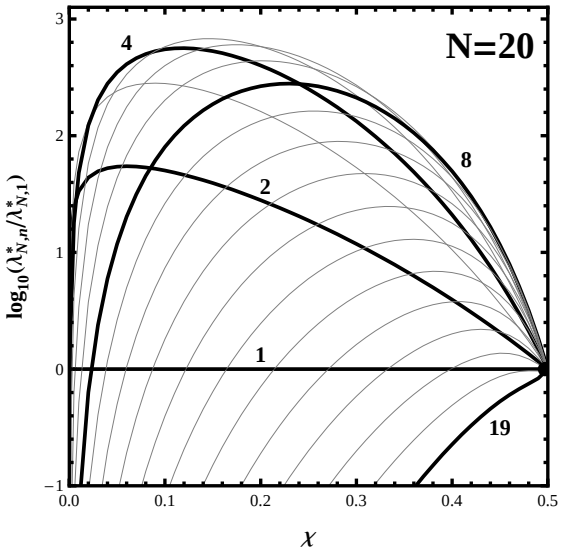

FIG. 11: Values of $\lambda^*_{N,n}/\lambda^*_{N,1}$, plotted as functions of χ for $N = 20$ and $1 \leq n \leq 19$. The curves corresponding to $n = 1, 2, 4, 8, 19$ are highlighted and labeled; the rest are not highlighted but proceed in sequential order relative to those which are. For $\chi \approx 0.05$, we see that the $n = 2$ vacuum has the highest value of $\lambda^*_{N,n}$, while it is the $n = 4$ vacuum which has this property for $\chi \approx 0.45$. The upper "envelope" of all of these curves corresponds to the critical stability value λ^*_N for the vacuum tower as a whole. Note that all of these curves converge to $\lambda^*_{N,n} = \sqrt{2^{N-1}/3}$ at $\chi = 1/2$.

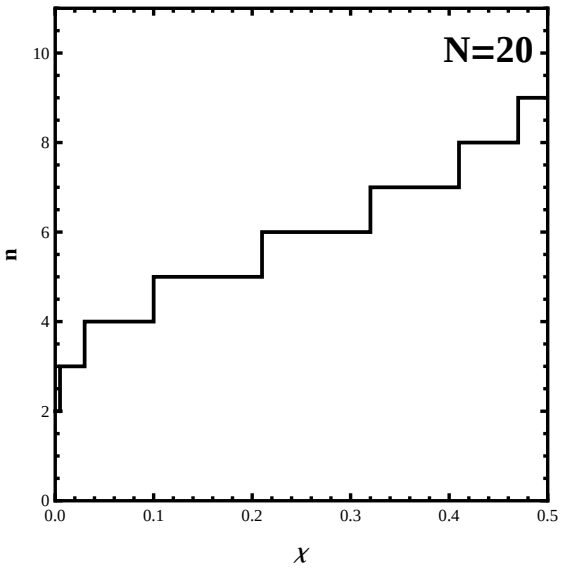

FIG. 12: The n-index of the vacuum with the largest corresponding critical value $\lambda^*_{N,n}$, plotted as a function of χ. This index specifies which vacuum in the tower is the first to destabilize as λ is lowered from infinity. In general, for large N, this index shifts from $n = 1$ to $n = [N/2]$ (where [x] is the greatest integer $\leq x$) as χ increases within the range $0 < \chi < 1/2$.

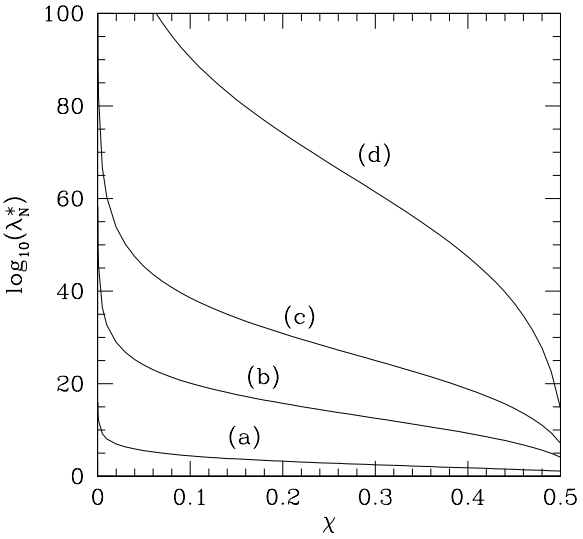

FIG. 13: The critical values λ^*_N, plotted as functions of χ for (a) $N = 10$, (b) $N = 30$, (c) $N = 50$, and (d) $N = 100$. We observe that λ^*_N generally grows with N, diverging as $\chi \to 0$ and asymptoting to $\sqrt{2^{N-1}/3}$ as $\chi \to 1/2$. We stress that the λ-values plotted here are the *rescaled, dimensionless* versions of our original Wilson-line coefficients. As such, there is no conflict with the perturbativity of our model.

Moreover, as already anticipated from the $N = 3$ and $N = 4$ special cases, λ^*_N always diverges as $\chi \to 0$ and asymptotes to $\lambda^*_N \to \sqrt{2^{N-1}/3}$ as $\chi \to 1/2$. The fact that λ^*_N diverges as $\chi \to 0$ for every N indicates that kinetic mixing plays a critical role in keeping our metastable vacuum tower stable.

We also stress that the λ-values plotted in Fig. 13 are the *rescaled, dimensionless* versions of our original Wilson-line coefficients. Indeed, they are only rescaled variables, not to be confused with our primordial Lagrangian couplings; indeed, as discussed earlier, this rescaling absorbs powers of the underlying gauge coupling g and the Fayet-Iliopoulos coefficient ξ. This rescaling is thus partly responsible for the rise in λ^*_N as a function of N. However, having such large values of λ naturally begs the question as to whether the stability of our vacuum towers is in conflict with the assumed perturbativity of our model. However, as we shall see below, there is no conflict between the two, and indeed such large values of the rescaled λ do not in and of themselves undermine the validity of our tree-level calculations.

D. Perturbativity and Mass Scales

The results obtained thus far have rested on the assumption that the physics of our model is perturbative at all relevant scales and is therefore accurately approximated by tree-level calculations. However, the true vacua

of our theory are those field configurations which minimize the *full* effective potential $V_{\rm eff}(\phi_i)$, and this includes radiative corrections. Thus, the tower of metastable vacua which we have presented above is guaranteed to be an accurate description of the actual vacuum structure of our model if and only if such corrections are small and $V_{\rm eff}(\phi_i) \approx V_{\rm tree}$, with $V_{\rm tree}$ given in Eq. (8). Indeed, this must hold within the vicinity of the solution to the classical potential for each applicable vacuum index n.

We will now demonstrate that there is no problem satisfying all applicable perturbativity constraints, provided the gauge coupling g is taken to be sufficiently small. Moreover, since small g is also beneficial for stabilizing the vacua in the tower, we shall find that there is no conflict between the constraints stemming from perturbativity and those stemming from vacuum stability — even as $N \to \infty$.

Note that in this subsection only, we shall revert back to our original *un*rescaled dimensionful parameters in order to expose the explicit dependence of our physical quantities on the gauge coupling g. This will restore factors of g and ξ in many of our previous expressions. For example, in terms of the original unrescaled dimensionful quantities λ and ξ, our expression for $\lambda^*_{N,n}$ in Eq. (33) takes the form

$$\lambda^{*2}_{N,n} \;=\; y^n \,\frac{\Gamma(y)}{\Gamma(n+y)}\,\frac{R_n^{N-2}}{\chi(1+R_n)}\,g^2\,\xi^{2-N}\;. \qquad (36)$$

Similar modifications to other expressions occur as well.

It turns out that a great deal of information about the effective potential can be gleaned from non-renormalization theorems [15]. For example, in supersymmetric field theories, the superpotential is not renormalized by perturbative effects, except via wavefunction renormalization. Moreover, this holds true even when the superpotential includes non-renormalizable operators [16]. As a result of such theorems, we expect corrections to V_F to arise only at scales near or below the supersymmetry-breaking scale $g\sqrt{\xi}$. However, these are typically the energy scales in which we are interested. Moreover, corrections to the Kähler potential do not, in general, vanish in supersymmetric theories. Thus, it will be necessary to discuss both sorts of corrections.

We begin by addressing radiative corrections to the Kähler potential. These arise due to diagrams which contribute to wavefunction renormalization of the various fields in the theory, and depend on g. For our purposes, it will be sufficient to focus on one-loop radiative corrections to the ϕ_i propagator; the contributing diagrams are then shown in Fig. 14. Let us begin by considering the contribution from diagrams with scalars running in the loop. There are $N+1$ such diagrams, and they result in a net contribution

$$\sum_j^{N+1} \frac{g^2}{16\pi^2}\,T_{ij}\,m_j^2\,\ln\left(\frac{m_j^2}{\mu^2}\right) \qquad (37)$$

where m_j is the mass of ϕ_j, where μ is an arbitrary renormalization scale, and where

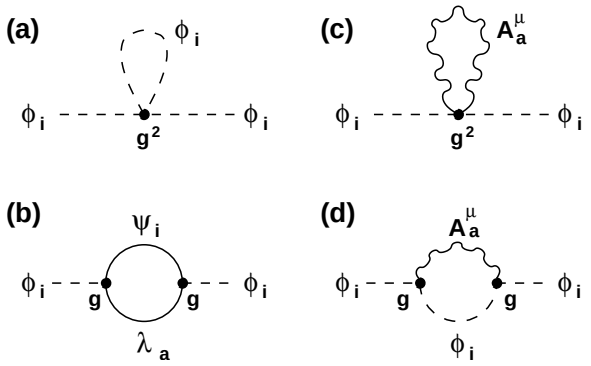

FIG. 14: Diagrams contributing to the wavefunction renormalization of ϕ_i at one loop. Each of these diagrams is proportional to g^2. Diagram (a) arises due to the quartic couplings in the D-term potential, while diagrams (b), (c), and (d) arise due to gauge-interaction terms for the scalars and the supersymmetrization thereof.

$$T_{ij} \;\equiv\; \sum_{a=1}^{N} \hat{Q}_{ai}\hat{Q}_{aj}\;. \qquad (38)$$

If T_{ij} were an arbitrary matrix, the expression in Eq. (37) would scale roughly as $N+1$ for large N, and the theory would rapidly become non-perturbative.

This is not the case, however, due to certain properties of T_{ij} which are essentially consequences of the moose structure of the model. In particular, all entries along the diagonal of this matrix are positive and $\mathcal{O}(1)$. Likewise, all elements with $i \neq j$ satisfy $-1 < T_{ij} < 0$, and the sum of elements in any row or column of T vanishes. Together, these properties imply that the contribution to the renormalization of the Kähler potential from scalar loops is essentially independent of N. Moreover, each of the additional diagrams in Fig. 14 yields a contribution to the two-point function for ϕ_i which is roughly of the order of T_{ii} (no sum on i). This is also essentially independent of N. Consequently, the renormalization of the Kähler potential is under control, and radiative corrections of this sort can be safely neglected as long as $g \ll 4\pi$ — even for very large N.

The second class of diagrams we must consider are corrections to the $2N$-field couplings in V_F which come from the terms in V_D. In other words, these are corrections to the superpotential coupling λ which arise from non-zero g. The leading such contribution arises at one-loop order from diagrams of the sort depicted in Fig. 15, along with additional diagrams in which gauge bosons and gauginos run in the loop. Note that similar diagrams were examined in Ref. [17]. In the limit of unbroken supersymmetry, of course, these contributions would sum to zero.

Each of the contributing diagrams of the sort pictured in Fig. 15 contains N vertices, and each of these vertices contributes a factor of $g^2 T_{ij}$ as well as N scalar propaga-

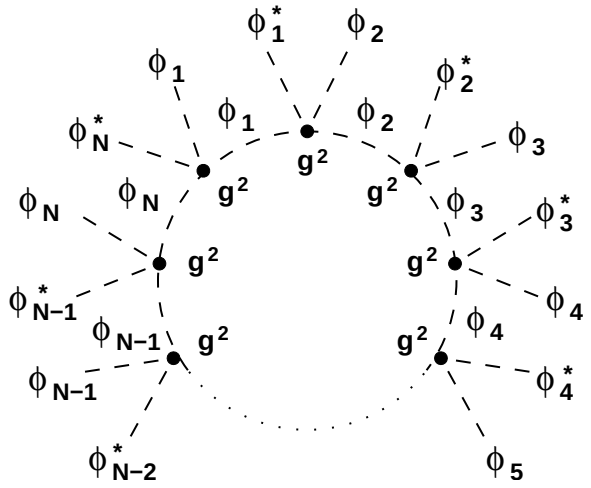

FIG. 15: A representative of the class of diagrams which contribute to the renormalization of the effective $2N$-scalar vertex at one loop in the broken phase of the theory, due to quartic D-term interactions. The diagram contains N vertices (each proportional to g^2) and N scalar propagators (with masses proportional to $g^2\xi$); the overall contribution is thus proportional to g^2.

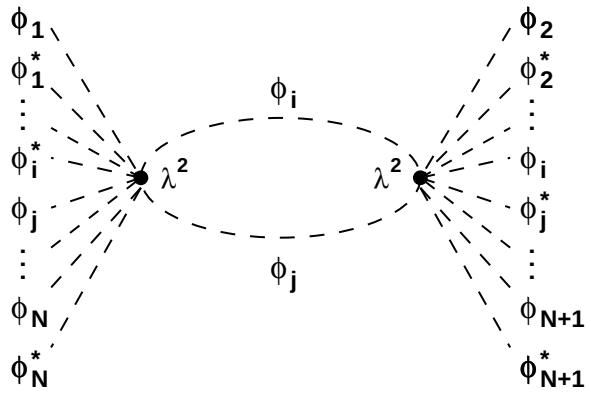

FIG. 16: A representative of the class of diagrams which contribute to the renormalization of the effective $2N$-scalar vertex at one loop in the broken phase of the theory, due to F-term interactions. This diagram represents a $4N-4$-scalar vertex in which $2N-4$ of the scalars on the external lines are assigned VEV's, and its contribution is proportional to λ^4. At high energies, when supersymmetry is effectively unbroken, this diagram is cancelled by the contribution from the diagram in Fig. 17.

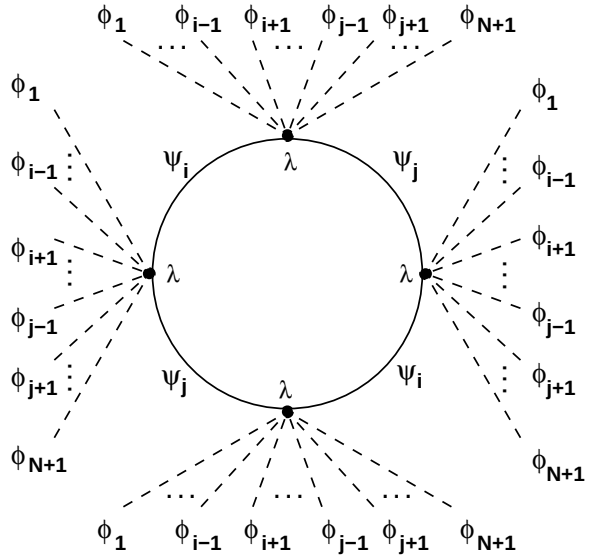

FIG. 17: A representative of the class of diagrams which correct the effective $2N$-scalar vertex at one loop. The net contribution from this class of diagrams would exactly cancel the contribution from the class of diagrams depicted in Fig. 16 if supersymmetry were unbroken.

tors. In any n-vacuum, the scalar masses are expected to be $\sim \mathcal{O}(g^2\xi R_n^{-1})$, so each diagram is proportional to g^2. There are $N! \sim N^N$ such diagrams, but each is proportional to $\mathrm{Tr}[T_{i_1 i_2} T_{i_2 i_3} \ldots T_{i_{N-1} T_N}]$ and hence suppressed by a factor of $T_{ij}^N \sim (1/N)^N$, where $i \neq j$. Thus, as was the case with the wavefunction-renormalization calculation above, the N-dependence essentially cancels. Thus, as long as $g \ll 4\pi$, this contribution too can be neglected — regardless of the value of N. By the same token, contributions to other effective operators which involve couplings of various numbers of scalar fields can also be safely neglected.

The final category of radiative corrections we must consider are corrections to the effective $2N$-scalar couplings, each of which has the tree-level coefficient λ^2. Thus, these are essentially corrections to the superpotential coefficient λ which themselves depend on λ. The leading contribution arises at one-loop order from diagrams of the form shown in Fig. 16, in which $2N-4$ fields are replaced by their VEV's, chosen appropriately for a given vacuum. However, along with these contributions we must also include the contributions from diagrams of the form shown in Fig. 17, also with VEV's assigned to an appropriate number of external fields. Again, these contributions cancel in the limit of unbroken supersymmetry, but their contributions can be expected to survive below the supersymmetry-breaking scale.

In the n-vacuum, the one-loop contribution to the $(\prod_{i=1}^{N+1} |\phi|^2)/|\phi_\ell|^2$ vertex from a given diagram of the sort shown in Fig. 16 is roughly

$$\frac{\lambda^4}{16\pi^2}\, P_{ijq}\, f(m_i^2, m_j^2)\, \frac{\prod_{k=1}^{N+1} v_k^2}{v_{N+1}^2 v_{N-n+1}^2 v_q^2}\ . \qquad (39)$$

Here $f(m_j^2, m_j^2)$ is a function of the masses m_i^2 and m_j^2 whose dependence on these masses is essentially logarithmic, while q denotes the index of the third scalar field ϕ whose VEV is missing from the contribution arising from the particular diagram in question. Likewise, P_{jkq} is a combinatorial factor representing the number of ways of assigning the appropriate VEV's to the external fields. Roughly speaking, we find that $P_{jkq} \sim 2^{N+1}$ for all (j,k,q). Similarly, there are $\sim (N-2)(N-1)$ di-

agrams which contribute at one-loop order to any given $2N$-scalar vertex.

Since the product of VEV's in Eq. (39) also appears in Eq. (36), we may rewrite our results directly in tems of $\lambda^*_{N,n}$. Thus, we find that this correction will be small compared to the tree-level term in any particular n-vacuum as long as

$$\frac{g^2}{16\pi^2}\,2^{N+1}\,(N-1)(N-2)\,\frac{\lambda^4}{(\lambda^*)^2}\,c_f \;\ll\; \lambda^2\;. \qquad (40)$$

Here c_f is an $\mathcal{O}(1)$ coefficient which embodies the effect of including the various $f(m_i^2, m_j^2)$ functions.

We recall, however, that we must also satisfy Eq. (7) in order to guarantee the stability of our entire vacuum tower. Thus, combining these two results, we find that the conditions under which both perturbativity and vacuum-stability constraints are simultaneously satisfied are given by

$$1 \;<\; \left(\frac{\lambda}{\lambda^*_N}\right)^2 \;\ll\; \frac{16\pi^2}{2^{N+1}g^2(N-1)(N-2)c_f}\;. \qquad (41)$$

Thus, there is no problem satisfying these two inequalities simultaneously provided

$$g^2 \;\ll\; \frac{16\pi^2}{2^{N+1}(N-1)(N-2)c_f}\;. \qquad (42)$$

We observe that this is also consistent with our previous constraint that $g \ll 4\pi$.

We conclude, then, that as long as the gauge coupling g satisfies Eq. (42) and λ lies within the range specified in Eq. (41), our model will remain perturbative for arbitrary N without compromising the stability of the vacuum tower. As a result, the tree-level results we have presented above are robust against quantum corrections. Of course, we observe that the required values of g tend to be rather small when N becomes large. However, N need not necessarily be taken large for all possible phenomenological applications. Moreover, situations in which N is taken to be extremely large tend to be higher-dimensional deconstruction-type scenarios in which we would naturally expect our four-dimensional gauge coupling to take an extreme value. Indeed, it is not unnatural to expect that the fine-tuning inherent in whatever drives $N \to \infty$ can also simultaneously drive $g \to 0$. Unfortunately, the details of such a mechanism lie within the full physical framework into which such a model is ultimately embedded, and thus requires a UV completion before they can be adequately addressed.

Our purpose here, however, has been to demonstrate that there exists a window in which both perturbativity and stability constraints can be simultaneously satisfied for any value of N. As we see from the above discussion, this is indeed the case.

Given these observations, it is interesting to investigate the degree to which our model can be considered natural. For a given choice of model parameters, and for all $N > 2$, this model contains two dimensionful parameters: the Wilson-line coefficient λ and the Fayet-Iliopoulos term ξ. Clearly, we can associate a mass scale with each of these parameters, defining μ_λ and μ_ξ such that $\lambda \equiv \mu_\lambda^{2-N}$ and $\xi \equiv \mu_\xi^2$. If we assume that ξ and λ are generated at the same underlying scale μ by the same physics, then our model can be considered natural from an effective field theory point of view as long as $\lambda = c_\lambda \mu^{2-N}$ and $\xi = c_\xi \mu^2$, where c_λ and c_ξ are both $\mathcal{O}(1)$ coefficients. We shall take this to be our definition of naturalness from an effective field theory point of view [18].

The question that arises, then, is whether our model meets this criterion. Recall that in our model, the particular values chosen for λ and ξ are constrained by the vacuum stability and perturbativity requirements embodied in Eq. (41), which in turn depend on the underlying model parameters primarily through λ^*_N. When written in terms of the scales μ_λ and μ_ξ, this quantity (in rescaled variables) is proportional to

$$\lambda^*_N \;\propto\; \frac{1}{g}\left(\frac{\mu_\xi}{\mu_\lambda}\right)^{N-2} \;=\; \frac{1}{g}\,c_\lambda\,c_\xi^{N/2-1}\;. \qquad (43)$$

Note, in particular, that this expression contains c_ξ taken to the $N/2-1$ power. As a result, the extremely large values of our rescaled dimensionless λ which are required for vacuum stability are not in conflict with either perturbativity constraints or naturalness considerations. Indeed, all that is required is that c_ξ be slightly larger than (but still of order) one.

III. DYNAMICS ON THE VACUUM TOWER: CASCADES, COLLAPSES, GREAT WALLS, AND FORBIDDEN CITIES

We now turn to the issue of dynamics within the metastable vacuum tower. What will be the pattern of tunneling-induced vacuum decays along the entire length of this tower?

Let us begin by recalling the simpler situation that arises if we have only two vacua separated by a single saddle-point barrier, with one vacuum state having higher vacuum energy than the other. In such a situation, the state with higher energy can decay to the state with lower energy via instanton transitions, the rate (per unit volume) for which may be parametrized as [19]

$$\frac{\Gamma_{\rm inst}}{\rm Vol} \;=\; A\,e^{-B}\;. \qquad (44)$$

We will not be particularly concerned with the form of the coefficient A. Instead, we will focus our attention on the exponent $B \equiv S_E(\phi_+, \phi_-)$, usually referred to as the *bounce action*, which represents the Euclidean action evaluated along the classical path in field space which connects ϕ_+, the field-space location of the higher-energy vacuum state, to ϕ_-, the field-space location of the lower-energy vacuum state, through the field-space

location of the saddle point between them. In general, one can evaluate B as in Ref. [20] by approximating the potential along the classical path between the two vacua as a triangle. In this approximation, the bounce action depends on four parameters: $\Delta\phi_\pm$, which is the distance in field space between the top of the potential barrier and the higher-energy (+) or lower-energy (−) vacuum; and $\Delta V_\pm$, which is the potential difference between the top of the barrier and each respective vacuum state. Note that in a multi-dimensional field space, the use of these results also intrinsically embodies a further approximation, namely that the classical path of least action follows a trajectory in field space consisting of two straight-line segments (one from the higher-energy vacuum to the saddle point, and the second from the saddle point to the lower-energy vacuum). However, this turns out to be a reasonably good approximation.

Calculating B is then relatively straightforward [20]. When

$$\frac{\Delta\phi_-}{\Delta\phi_+} \;\geq\; \frac{\sqrt{1+c}+1}{\sqrt{1+c}-1} \tag{45}$$

with $c \equiv (\Delta V_-/\Delta V_+)(\Delta\phi_+/\Delta\phi_-)$, the bounce action is given by [20]

$$B \;=\; \frac{32\pi^2}{3g^2}\frac{1+c}{(\sqrt{1+c}-1)^4}\left(\frac{\Delta\phi_+^4}{\Delta V_+}\right) \;. \tag{46}$$

By contrast, when the inequality in Eq. (45) is not satisfied, the appropriate expression is instead given by [20]

$$B \;=\; \frac{\pi^2}{96g^2}\left(\frac{\Delta V_+}{\Delta\phi_+}\right)^2 R_T^3 \times\left(-\beta_+^3+3c\beta_+^2\beta_-+3c\beta_-^2\beta_+-c^2\beta_-^3\right) \;, \tag{47}$$

where $\beta_\pm$ and R_T are given by

$$\beta_\pm \equiv \left(\frac{8\Delta\phi_\pm^2}{\Delta V_\pm}\right)^{1/2} \;, \qquad R_T \equiv \tfrac{1}{2}\left(\frac{\beta_+^2+c\beta_-^2}{c\beta_--\beta_+}\right) \;. \tag{48}$$

It can be verified that these solutions match smoothly at the point where Eq. (45) is saturated.

Note that the factors of g^2 which appear in the denominators of Eqs. (47) and (48) arise from the fact that we are using rescaled energies $\Delta V_\pm$ and field-space distances $\Delta\phi_\pm$ in these expressions, in accordance with the discussion in Sect. II. In the following, we shall take $g = 1$ for simplicity in all numerical evaluations of the bounce action.

This is the situation that emerges when there are only two vacua to consider. However, in this paper we face a situation in which we have a whole tower of metastable vacua with many possible pairwise saddle-point solutions. The situation we face is therefore significantly more complicated than that sketched above.

In order to approach this situation, therefore, we begin with some preliminary observations. First, we observe that if we are interested in transitions between an initial vacuum n_i and a final vacuum n_f, we need only consider the leading quantum-mechanical transition amplitude $\langle n_f|n_i\rangle$, corresponding to the bounce action $B(n_i,n_f)$. Although higher-order quantum-mechanical contributions of the form $\sum_n\langle n_f|n\rangle\langle n|n_i\rangle$ can appear when there are more than two vacua, such contributions are all exponentially suppressed. It is therefore sufficient to examine the bounce action $B(n_i,n_f)$ itself in order to determine the transition rate between two specified vacua n_i and n_f.

Second, we observe that in general, a given initial vacuum state n_i can decay into all possible final vacuum states n_f, where $n_i < n_f \leq N-1$. As a quantum-mechanical issue, of course, all of these transitions take place simultaneously, with rates determined by the corresponding bounce actions $B(n_i,n_f)$. However, once again, these transition rates will typically experience huge, exponential variations as functions of the possible value n_f. Indeed, this will be the situation for all $0<\chi<1/2$. As a result, we shall make a "classical" approximation in which each vacuum state n_i is assumed to decay to the unique final vacuum n_f for which $B(n_i,n_f)$ is minimized, with a rate determined by $B(n_i,n_f)$.

Third, in order to evaluate $B(n_i,n_f)$, we shall need explicit expressions for the energies of the n_i- and n_f-vacua as well as the height of the saddle-point barrier which connects them. We shall also require the field-space separations between the two vacua and the saddle point. While analytical expressions for these vacuum configurations exist (and were given in Sect. II), we do not have analytical expressions for the saddle-point configurations except in the "asymptotic" $\lambda\to\infty$ limit. Therefore, although we will *not* assume that λ is actually infinite in what follows, we *shall* assume that λ is sufficiently large that the asymptotic saddle-point solutions given in Sect. II may be utilized without significant error. As we have already seen in Sect. IID, this assumption is not necessarily in conflict with the presumed perturbativity of our model; indeed, the approach to the asymptotic limit was sketched for the $N=3$ case in Fig. 4, whereupon we observe that the large-λ asymptotic behavior emerges even for relatively small values of λ. The assumption of the large-λ limit will also have the added advantage of removing the free variable λ from the subsequent analysis.

Finally, we shall deem a metastable vacuum to be "stable" if its lifetime exceeds the age of the universe. More precisely, we demand a lifetime of such magnitude that no decay event would be expected within our Hubble volume over a duration equal to the known age of the universe ≈ 13.7 Gyr. Using Eq. (44), we can package this requirement as a constraint on the bounce action:

$$B \;\gtrsim\; 471 \;+\; 4\,\ln\left(\frac{M_{\rm inst}}{M_{\rm Planck}}\right) \;, \tag{49}$$

where $M_{\rm inst}\equiv A^{1/4}$. When this constraint is satisfied, the corresponding vacuum in question is stable on cosmological time scales; when it is not, the vacuum is as-

sumed to have decayed sometime in the past. In what follows, we will adopt the most conservative assumption that $M_{\rm inst} \approx M_{\rm Planck}$, whereupon the logarithmic contribution in Eq. (49) can be ignored. Thus, $B \approx 471$ shall serve as our critical bounce action for stability.

Given these assumptions, it is then possible to examine the corresponding decay patterns along our entire metastable tower. To do this, we need to understand the behavior of the bounce actions $B(n_i, n_f)$ as functions of n_i and n_f as we vary our two remaining variables, χ and N. As we shall see, there are two principal modes of possible behavior patterns ("collapse" and "cascade") which will emerge.

A. Collapse behavior

To understand how these two different patterns arise, let us begin our analysis by revisiting the simple $N = 4$ case discussed in detail in Sect. IIB. For $N = 4$, the vacuum tower contains three minima (the $n = 1$, $n = 2$, and $n = 3$ vacua), and hence three different decay transitions are possible. The bounce actions $B(n_i, n_f)$ associated with these three transitions are plotted in Fig. 18 as functions of χ.

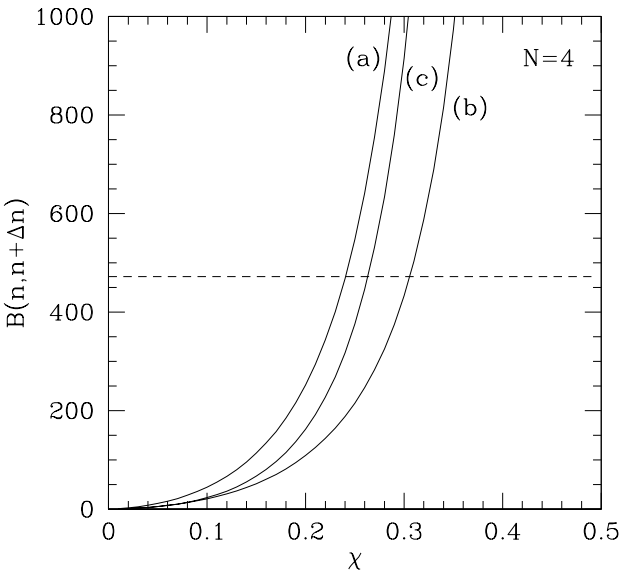

FIG. 18: Bounce actions for the $N = 4$ model, plotted as functions of χ. In each case we have plotted $B(n, n + \Delta n)$ where (a) $(n, \Delta n) = (1, 1)$, (b) $(n, \Delta n) = (1, 2)$, and (c) $(n, \Delta n) = (2, 1)$. Also shown (dotted line) is the bounce action corresponding a decay lifetime approximating the age of the universe. In general, all bounce actions increase with increasing χ, ultimately diverging as $\chi \to 1/2$. However, for each value of χ, we see that the bounce actions corresponding to the greatest Δn are smaller than those corresponding to smaller Δn.

This figure illustrates several general trends. First, we observe the

- *General feature #1:* All of our bounce actions vanish as $\chi \to 0$ and diverge as $\chi \to \infty$.

This feature is easy to understand. As $\chi \to 0$, our entire vacuum tower becomes unstable, whereupon all of the possible decays out of any given vacuum state become essentially instantaneous. Likewise, as $\chi \to 1/2$, the vacuum energy differences between any two vacua in the tower vanish. There is thus no "driving force" for decays in the $\chi \to 1/2$ limit, whereupon the lifetime of any given metastable state approaches infinity and the states become truly stable with respect to instanton-tunnelling transitions.

Second, we observe from Fig. 18 that $B(2, 3) < B(1, 3) < B(1, 2)$ for all χ. This implies that the $n = 1$ vacuum decays preferentially *not* to the $n = 2$ metastable state immediately below it, but directly to the $n = 3$ ground state. Moreover, if both the $n = 1$ and $n = 2$ vacua were somehow initially occupied (*e.g.*, in the different regions of the universe), we find that the $n = 2$ region would decay to the ground state before the $n = 1$ vacuum region does.

These observations are examples of two additional general features:

- *General feature #2:* A given bounce action $B(n, n+\Delta n)$ tends to decrease with increasing n if Δn is held fixed.

- *(Nearly) general feature #3:* A given bounce action $B(n, n+\Delta n)$ tends to decrease with increasing Δn if n is held fixed. (Important exceptions will be discussed below.)

Both of these features are illustrated for the $N = 20$ model in Fig. 19, where we plot the values of the bounce actions $B(n, n + \Delta n)$ as functions of n for a variety of fixed Δn.

These features also have direct physical consequences. For example, Feature #3 implies that each metastable vacuum in our tower tends to decay directly to the ground state of the theory rather than to any other metastable state of lower energy. We shall refer to this type of behavior as a "collapse": each state, one at a time, suddenly drops directly to the ground state with $n = N - 1$. As we shall discuss below, Feature #3 (and thus the ensuing collapse behavior) tends to hold for most values of N and χ; indeed, the only exceptions tend to arise in the $\chi \to 0$, $N \to \infty$ limit, with both $n, \Delta n \ll N$. Thus, collapse behavior tends to dominate along the full length of most metastable vacuum towers, and along the lower portions of all towers even when $\chi \to 0$ and $N \to \infty$.

If we imagine situations in which all vacuum states are initially populated (*e.g.*, in different regions of the universe), the specific collapse pattern along the metastable vacuum tower becomes of particular interest. To address this issue, we cannot hold n or Δn fixed; we must vary

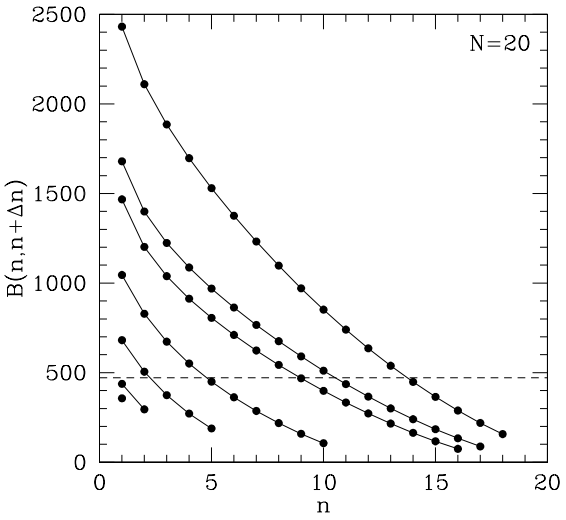

FIG. 19: Bounce actions for the $N = 20$ theory with $\chi = 1/5$. For each vacuum $1 \leq n \leq 18$, we plot $B(n, n + \Delta n)$ where the different "curves" (from top to bottom) correspond to $\Delta n = 1, 2, 3, 9, 14, 17, 18$ respectively. Note that each plot is truncated when $n + \Delta n$ would exceed $n_{\rm max} = 19$. We observe that for fixed n, the bounce action $B(n, n + \Delta n)$ generally decreases with increasing Δn. As a result, for fixed n, transitions which maximize Δn are generally favored.

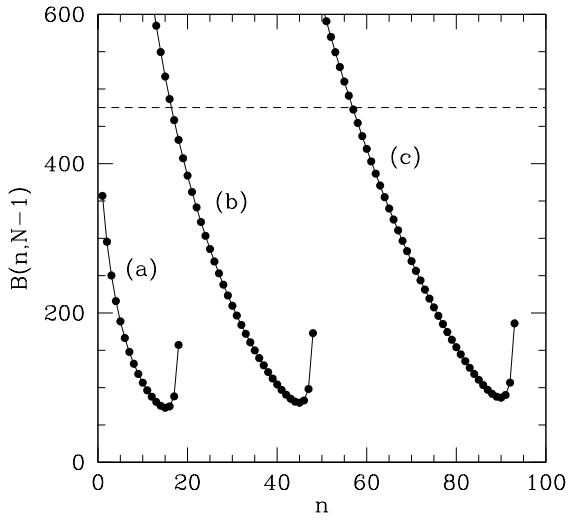

FIG. 20: Bounce actions $B(n, N-1)$ with $\chi = 1/5$, plotted as functions of n for (a) $N = 20$, (b) $N = 50$, and (c) $N = 95$. In each case, the vacua which populate the lower portions of each vacuum tower eventually decay by tunneling directly to the true ground state. However, the first metastable vacuum to decay in this manner is *not* the first excited vacuum; instead, these decays follow a complicated collapse pattern, with different portions of the vacuum tower decaying at different times. By contrast, for sufficiently large N, the vacua populating the upper portions of our vacuum towers have lifetimes exceeding the age of the universe, corresponding to the critical bounce action $B \approx 471$ (dotted line).

both simultaneously in order to hold $n_f = n + \Delta n = N - 1$ fixed. In other words, we wish to examine the bounce action $B(n, N-1)$ as a function of n.

This behavior is shown in Fig. 20 for $N = 20$, 50, and 95. In each case, we see that the vacua which populate the lower portions of each vacuum tower tend to decay first. However, we also see that the first metastable vacuum to decay is *not* the first excited vacuum with $n = N - 2$; instead, these decays follow a complicated collapse pattern, with different portions of the vacuum tower decaying at different times. For example, in the case with $N = 20$ and $\chi = 1/5$ shown in Fig. 20(a), we see that the first vacuum to decay into the ground state with $n = 19$ is actually the $n = 15$ vacuum. The vacua then decay sequentially, with decreasing values of n, except that the $n = 16$ vacuum decays between the $n = 15$ and $n = 14$ vacua, the $n = 17$ vacuum decays between the $n = 12$ and $n = 11$ vacua, and the $n = 18$ vacuum decays between the $n = 6$ and $n = 5$ vacua.

As N increases, this behavior persists. Ultimately, however, we find that our collapse pattern develops a new feature: an *upper critical location* on the tower above which our vacua remain stable on cosmological time scales. For example, we see from Fig. 20(b) that for $N = 50$, the collapse pattern begins with the $n = 45$ vacuum decaying first. The avalanche of collapses ultimately spreads up the tower until it reaches the $n = 16$ vacuum, at which point it stops. Thus, the vacua with $n \leq 16$ remain stable.

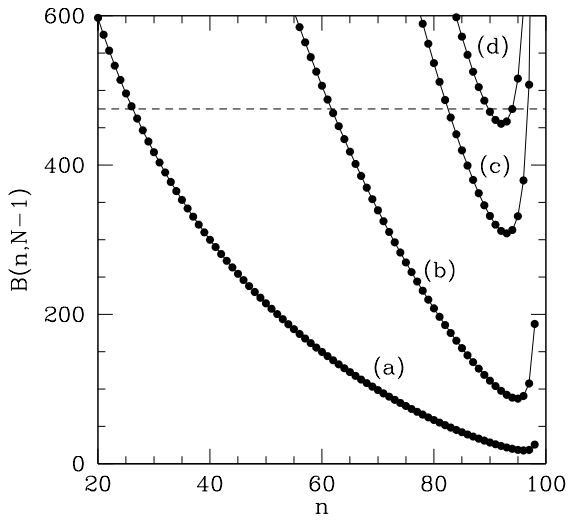

FIG. 21: Bounce actions $B(n, N-1)$ for $N = 100$, plotted as functions of n for (a) $\chi = 0.1$, (b) $\chi = 0.2$, (c) $\chi = 0.3$, and (d) $\chi = 0.33$. The critical bounce action (dotted line) corresponds to lifetimes exceeding the age of the universe. In general, we see that only a narrow band of metastable vacua within the vacuum tower will take part in the collapse pattern and decay to the ground state; by contrast, vacua above or below this band in the vacuum tower will generally remain stable. As the kinetic mixing parameter χ increases towards its maximum value 1/2, this collapse band grows increasingly narrow and ultimately disappears.

The above results apply for relatively small values of χ. However, as χ increases, our wave of collapses develops a *lower limit* as well. This behavior is shown in Fig. 21. For example, we see from Fig. 21(c) that for $N = 100$ and $\chi = 0.3$, the avalanche begins with the $n = 93$ vacuum and spreads up the tower to the $n = 83$ vacuum before stopping. However, it only spreads down the tower to the $n = 96$ vacuum, where it stops as well. Indeed, vacua with $n \leq 82$ and $n = 97, 98$ are stable. In general, as the kinetic mixing parameter χ increases towards its maximum value $1/2$, this avalanche band grows increasingly narrow and ultimately disappears. This is consistent with Feature #1 that lifetimes along the vacuum tower diverge as $\chi \to 1/2$.

We also note from Fig. 20 that

- *General feature #4:* For fixed n_i and n_f, a given bounce action $B(n_i, n_f)$ tends to increase with N.

This is a direct consequence of the fact that even when n_i and n_f are held fixed, the corresponding distance in field space between the n_i- and n_f-vacua increases with N because the dimensionality of the field space itself increases with N. Since the energies of the n_i- and n_f-vacua are N-independent, the lifetime of the n_i-vacuum increases.

B. Cascade behavior

As we have seen, it is Feature #3 which is directly responsible for the "collapse" behavior in which each metastable vacuum state decays directly into the true ground state of the theory rather than into another metastable ground state. However, as we shall now discuss, Feature #3 is not generally valid, and indeed the resulting behavior tends to change rather dramatically in the $\chi \to 0$, $N \to \infty$ limit.

To understand the emergence of this qualitatively new behavior, let us consider the $\chi \to 0$, $N \to \infty$ limit analytically. We then find that the quantities which determine our bounce actions have the leading behavior

$$\begin{aligned}
\Delta V_+ &\sim \frac{1}{2n_i^2(n_f - n_i)}\,\chi^2 + \mathcal{O}(\chi^3) \\
\Delta V_- &\sim \frac{n_f - n_i}{2n_i n_f} + \mathcal{O}(\chi) \\
\Delta\phi_+ &\sim \frac{N}{n_i}\,\chi + \mathcal{O}(\chi^{3/2}) \\
\Delta\phi_- &\sim c_0 + c_1\chi^{1/2} + \frac{N}{n_f}\,\chi + \mathcal{O}(\chi^{3/2})
\end{aligned} \tag{50}$$

where we have assumed that $n_i, n_f \ll N$, and where c_0, c_1 are $\mathcal{O}(1)$ coefficients which generally decrease with n_i but increase approximately linearly with n_f. For example, $c_0 = (n_f - 1)/2$ for $n_i = 1$.

The results in Eq. (50) are easy to understand. As $\chi \to 0$, the saddle point between the n_i- and n_f-vacua shifts to join (and thereby destabilize) the n_i-vacuum; as a result, ΔV_+ and $\Delta\phi_+$ both vanish in this limit. However, as expected, ΔV_- and $\Delta\phi_-$ remain non-zero, even in this limit. We also observe from the above results that $\Delta V_\pm$ are N-independent, while all N-dependence lies within $\Delta\phi_\pm$. This too is expected.

Given these results, it is relatively straightforward to understand the leading behavior of $B(n_i, n_f)$ as $\chi \to 0$, $N \to \infty$. We see from Eq. (50) that there are two limiting cases to consider, depending on the value of $N\chi$. For $N\chi/n_f \ll c_0$, the leading term c_0 in $\Delta\phi_-$ dominates. In such cases, we find that the inequality in Eq. (45) is always satisfied, whereupon the bounce action $B(n_i, n_f)$ takes the approximate analytical form

$$B(n_i, n_f) \;\approx\; \frac{64 c_0 \pi^2}{3g^2}\,\frac{n_f}{n_i^2(n_f - n_i)}\,(N\chi)^3\;. \tag{51}$$

By contrast, for $N\chi/n_f \gg c_0$, it is the $N\chi/n_f$ term in $\Delta\phi_-$ which dominates. We then find that the inequality in Eq. (45) is never satisfied, in which case the bounce action $B(n_i, n_f)$ takes the approximate analytical form

$$B(n_i, n_f) \;\approx\; \frac{4\pi^2}{3g^2}\,\left(\frac{3n_f - n_i}{n_f - n_i}\right)\left(\frac{n_i + n_f}{n_i n_f}\right)^3\,(N\chi)^4\;. \tag{52}$$

Thus, for any value of $N\chi$, we see that the choice of whether Eq. (51) or Eq. (52) applies depends on how $N\chi$ compares with $c_0 n_f$. However, since c_0 itself grows approximately linearly with n_f, we see that the first case will apply for $n_f \gg n_f^*$, where

$$n_f^* \;\equiv\; \sqrt{N\chi}\;. \tag{53}$$

By contrast, the second case will apply for $n_f \ll n_f^*$. Also note that in either case, the actual value of $B(n_i, n_f)$ depends on the product $N\chi$. This is not unexpected. According to Feature #1, the bounce action should vanish as $\chi \to 0$, while it should diverge as $N \to \infty$ according to Feature #4. Thus, when both limits are taken simultaneously, it is not unreasonable that the bounce action depend on the product.

Given these results, we can now consider how $B(n_i, n_f)$ varies with n_f for fixed n_i in the limit as $\chi \to 0$, $N \to \infty$. In general, Eq. (51) is a *rising* function of n_f, while Eq. (52) is a *falling* function. As a result, we expect that as $B(n_i, n_f)$ for fixed $N\chi$ should generally develop a dip (or "trough") centered around n_f^* as $\chi \to 0$, $N \to \infty$. This behavior is shown in Fig. 22, where we plot the normalized bounce actions $B(1, n_f)/B(1, 2)$ as functions of n_f in the allowed range $2 \leq n_f \leq N - 1$. In this figure, we have taken $\chi = 1/10$ and we vary N from $N = 10$ to $N = 10^4$. As N increases, we see from Fig. 22 that our bounce-action function indeed develops a deepening trough whose minimum is approximately located at $n_{f*} \equiv \sqrt{N\chi}$. This, then, is a counter-example to Feature #3.

This does not, however, eliminate the resulting collapse behavior. As long as the minimum bounce action along

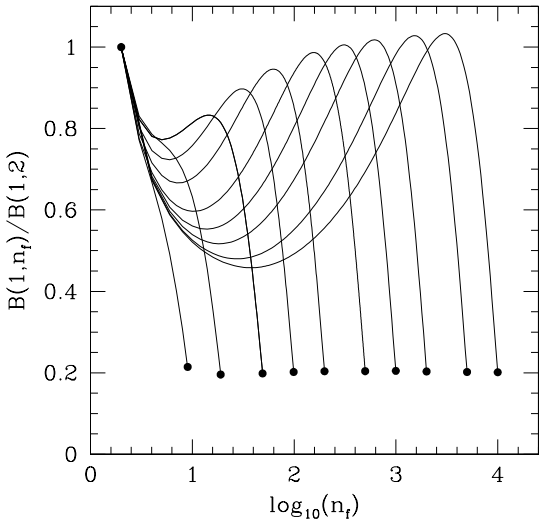

FIG. 22: Normalized bounce actions $B(1, n_f)$ with $\chi = 1/10$, plotted as functions of n_f in the allowed range $2 \leq n_f \leq N-1$. The curves whose lower portions progress from left to right correspond to ordered increasing values of $N \in \{1, 2, 5\} \times 10^{\{1,2,3\}}$, ending with $N = 10^4$. We observe that as N increases, the bounce actions $B(1, n_f)$ develop a deepening "trough" whose minimum is approximately located at $n_f \approx n_f* \equiv \sqrt{N\chi}$. The depth of the trough asymptotes to a finite value as $N \to \infty$ in such a way that the minimum bounce action along any such curve corresponds to $n_f = N - 1$.

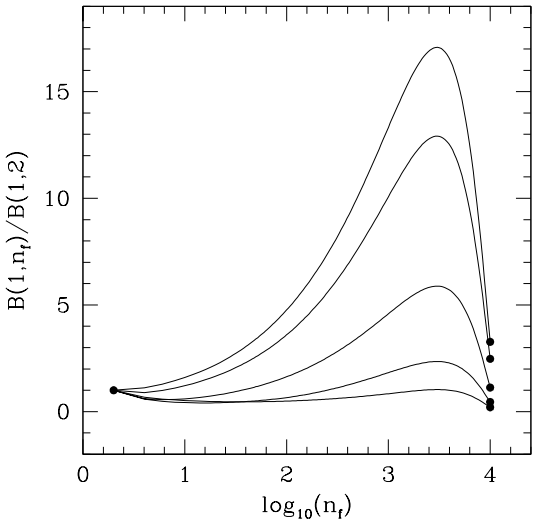

FIG. 23: The normalized bounce actions $B(1, n_f)$, plotted as functions of n_f in the allowed range $2 \leq n_f \leq N-1$, with $N = 10^4$. The different curves progressing from lowest to highest correspond to $\chi = 10^{-1}, 10^{-2}, 10^{-3}, 10^{-4}$, and 10^{-5}; note that the lowest curve here is the same as the $N = 10^4$ curve shown in Fig. 22. As $\chi \to 0$, we see that $n_f^* \to 0$; thus the bounce actions increasingly tend to *grow* as functions of n_f, at least for sufficiently small n_f. Also important is the fact that for sufficiently small χ, the bounce action at $n_f = N-1$ begins to *exceed* that at $n_f = 2$. For each such curve, the minimum bounce action therefore occurs *not* for $n_f = N-1$, but for $n_f = 2$. This triggers the onset of cascade (rather than collapse) behavior for our vacuum towers.

any individual curve continues to occur at the maximum value $n_f = N - 1$, the $n = 1$ vacuum (and indeed all n_i-vacua) will continue to preferentially decay directly to the $n_f = N - 1$ ground state. At first glance, one might suspect that taking even larger values of N in Fig. 22 would produce an even deeper trough which would eventually become deeper than the minimum bounce action at $n_f = N - 1$. However, as we see from Fig. 22, the depth of the trough actually approaches an asymptote as $N \to \infty$, and this asymptotic depth continues to exceed the $n_f = N - 1$ bounce action. Thus our collapse behavior remains undisturbed.

Of course, the above comments pertain to the situation in Fig. 22 for which we took $\chi = 1/10$. Such a value for χ — while suitable for illustrating the emergence of the trough — is still not yet small enough to alter the collapse behavior. The situation changes dramatically, however, if we take χ even smaller and enter the true $\chi \to 0$ regime. For any fixed N, we have seen from the above analysis that taking the $\chi \to 0$ limit has the effect of sliding $n_f^* \to 0$. We therefore expect that as $\chi \to 0$, the initially falling portion of the $B(n_i, n_f)$ curve should disappear, and $B(n_i, n_f)$ should actually begin to *rise* as a function of n_f (as long as $n_f \ll N$ and N is held fixed). This behavior is shown in Fig. 23, where we have held N fixed and plotted $B(1, n_f)$ as a function of n_f while we

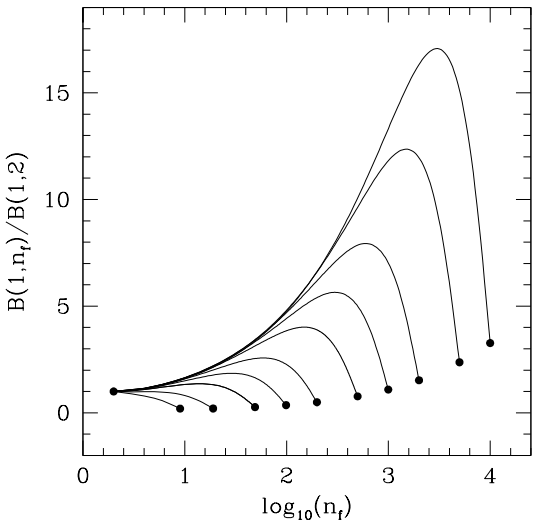

FIG. 24: Same as Fig. 22, except plotted for $\chi = 10^{-5}$ rather than $\chi = 1/10$. We observe that as N increases (approaching the true $N \to \infty$ limit), the minimum bounce action begins to occur for relatively small values of n_f rather than for $n_f = N-1$. As in Fig. 23, this triggers the onset of cascade (rather than collapse) behavior for our vacuum towers.

reduce χ from 10^{-1} to 10^{-5}. Thus, as we see from Fig. 23, reducing χ has the geometric effect of "uplifting" each of the curves in Fig. 22. Indeed, this uplifting is the generic behavior that occurs as we enter the true $\chi \to 0$ limit.

Given these results, we see that the net effect of reducing χ is that the behavior shown in Fig. 22 smoothly shifts to become the behavior shown in Fig. 24. Indeed, these two figures plot exactly the same bounce actions $B(1, n_f)$; the only difference between them is that the former is calculated with $\chi = 1/10$ while the latter is calculated with $\chi = 10^{-5}$. However, we now see that the effect of reducing χ has been dramatic: while the smallest bounce action $B(1, n_f)$ along any curve in Fig. 22 occurs for the *maximum* allowed value $n_f = N - 2$, the smallest bounce actions $B(1, n_f)$ along the curves with large N in Fig. 24 now occur for the *minimum* allowed value $n_f = 2$. Thus, while the top vacuum in our tower prefers to decay directly to the ground state when $\chi = 1/10$, it prefers to decay to merely the metastable vacuum immediately below it when N is sufficiently large and $\chi = 10^{-5}$!

Since the top vacuum has only decayed to another metastable state in the vacuum tower rather than to the ground state, the cycle can then repeat. In this case, for example, the nature of the subsequent vacuum decay now depends on the behavior of $B(2, n_f)$ as a function of n_f for $3 \leq n_f \leq N - 1$. However, as long as $n_i \ll N$, the same situation persists: the preferred subsequent decay is into the next-lowest vacuum, and the cycle repeats yet again. Thus, what emerges is not a collapse into the ground state, but rather a sequential *cascade* from vacuum to lower vacuum.

It should be stressed that not all vacuum cascades necessarily proceed through single-vacuum hops. Indeed, although this was the result emerging for the curves with the largest values of N plotted in Fig. 24, these curves still all correspond to cases with $N\chi < 1$. However, in the true $\chi \to 0$, $N \to \infty$ limit, the size of the cascade hops generally depends on the product $N\chi$. This is illustrated in Fig. 25, where we have plotted the values of $B(1, n_f)$ for different values of $N\chi$, all while remaining completely within the double $\chi \to 0$, $N \to \infty$ limit. As expected from our above analysis, increasing the value of $N\chi$ has the effect of increasing n_f^* and thereby shifting the minimum of the curve towards larger values of n_f. In such cases, the value of n_f which minimizes $B(n_i, n_f)$ will occur for $n_f = n_i + \Delta n$ where $\Delta n > 1$. As a result, for $N\chi \gg \mathcal{O}(1)$, cascades can often proceed through larger, multiple-vacuum hops, and indeed non-trivial cascade trajectories can easily develop. An explicit example of such a non-trivial cascade pattern will be presented below.

In general, even in the double $\chi \to 0$, $N \to \infty$ limit, vacuum cascades do not continue all the way down the vacuum tower. Instead, beyond a certain point, n_i becomes sufficiently large that the behavior of $B(n_i, n_f)$ as a function of n_f reverts back to the collapse pattern, with the minimum bounce action occurring for the ground state $n_f = N - 1$. Thus, a system which starts at the top of the tower eventually cascades down the tower to a critical level n^* at which collapse behavior takes over. The subsequent (and final) decay will then be directly to the ground state.

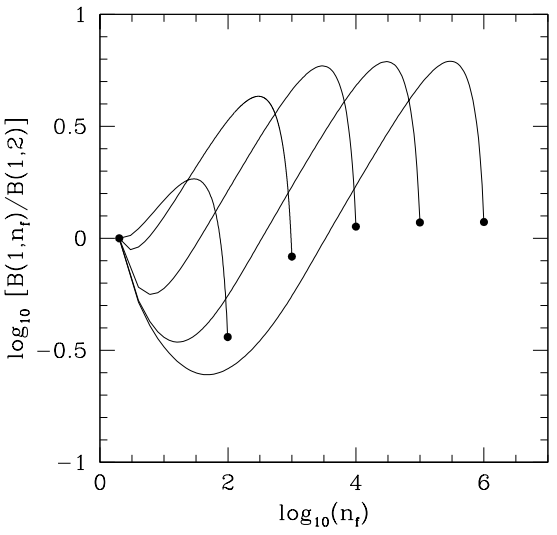

FIG. 25: Behavior of $B(1, n_f)$ as a function of of n_f in the allowed range $2 \leq n_f \leq N-1$, plotted for different values of $N\chi$. The curves whose end positions progress from left to right correspond to ordered increasing values of $N\chi = 10^{\{-1,0,1,2,3\}}$, where we have held $\chi = 10^{-3}$ fixed. As $N\chi$ increases, the bounce actions $B(1, n_f)$ develop a deepening "trough" whose minimum is approximately located at $n_f \approx n_f^* = \sqrt{N\chi}$. As a result, the vacuum cascade step size increases as a function of $N\chi$.

The critical value n^* at which cascade behavior becomes collapse behavior generally increases with N. In fact, we have found numerically that

$$n^* \;\approx\; cN \tag{54}$$

where $c \approx 2.32 \times 10^{-3}$. Remarkably, this relationship holds with increasing precision as N grows large. Moreover, this relationship is independent of χ. Of course, as discussed above, the mere existence of a cascade region already presupposes that we are in the $\chi \to 0$ limit. However, once χ is sufficiently small as to produce cascade behavior and establish a non-zero value of n^*, reducing χ still further will not increase n^* beyond this value. Indeed, only with a simultaneous increase in N can an increase in n^* be accomplished.

The result in Eq. (54) implies that for large N and small χ, *no more than the uppermost* 0.23% *of any given vacuum tower can experience cascade behavior as opposed to collapse behavior*. This small value presumably reflects the overall numerical coefficients which appear in the expressions for our bounce actions in Eq. (46); indeed, we observe that $c \sim \mathcal{O}(1/32\pi^2)$ as far as overall scales are concerned. Despite its small relative size, however, this cascade region of the vacuum tower is of tremendous im-

portance for two reasons:

- For large N, this region gives rise to the vast majority of the vacuum transitions that a given system can undergo — indeed this cascade region of the tower gives rise to literally *all* possible vacuum transitions for our system, except for the final transition to the ground state.
- Likewise, for any N, these vacuum transitions involve the greatest shifts in vacuum energy that the system can experience. Indeed, as we have seen in Sect. II, the differences in vacuum energy between neighboring vacua grow increasingly small as we move down the vacuum tower. Thus, for large N, essentially all of the original vacuum energy of our system is dissipated through vacuum transitions occurring in this region of the tower.

Thus, to summarize: in the double $\chi \to 0$, $N \to \infty$ limit, we find that a vacuum cascade can emerge near the top of our metastable vacuum towers. In general, the value of the product $N\chi$ governs the size of the hops taken in each step of this cascade. Eventually, the cascade proceeds down the tower until a critical value n^* is reached, at which point the cascade behavior reverts back to collapse behavior. This value of n^* increases with N, but is essentially independent of χ so long as we remain in the $\chi \to 0$ limit which was required to produce the cascade region in the first place. Moreover, n^* is always significantly less than N. As a result, there is always a substantial collapse region in the lower portion of any vacuum tower.

Finally, of course, we recall Feature #2 which asserts that bounce actions which govern the decays of vacua near the top of any vacuum tower generally exceed those near the bottom. As a result, it is possible that such bounce actions near the tops of our metastable vacuum towers will exceed the critical value $B \approx 471$ required for stability on cosmological time scales. As a result, it is possible that the uppermost vacua in any vacuum tower will be essentially stable.

C. An explicit example

To illustrate all of these decay patterns and features simultaneously within a single model, let us consider the specific example with $N = 5000$ and $\chi = 2.8 \times 10^{-4}$. Since this choice has $\chi \ll 1$ and $N \gg 1$, we see that it is precisely such a choice which will yield both a cascade region as well as a collapse region. Moreover, since $N\chi \sim \mathcal{O}(1)$, we expect that our vacuum cascade will proceed through relatively small steps.

A plot detailing the vacuum dynamics for this choice of parameters is shown in Fig. 26. For each n, we have plotted $B(n, n')$ for that value of n' ($n < n' \leq N - 1$) which minimizes $B(n, n')$ and which thereby indicates the next vacuum along the corresponding cascade trajectory. For example, we see from this figure that the $n = 3$ vacuum decays into the $n = 6$ vacuum, which in turn decays (even more rapidly) into the $n = 10$ vacuum; this in turn decays (even more rapidly) into the $n = 15$ vacuum, which in turn decays directly into the ground state. There are, of course, limits to this cascade region, both at the top and at the bottom. For example, the bounce actions for the top two vacua exceed our critical bounce action $B \approx 471$; these vacua, if initially populated, are consequently deemed stable on cosmological time scales. Likewise, at the $n = 11$ vacuum and beyond, we enter the collapse region in which all subsequent decays automatically proceed directly to the ground state.

Nevertheless, within the cascade region between the $n = 3$ and $n = 10$ vacua, we see that this model contains four independent potential cascade trajectories, each of which unfolds with increasing speed (*i.e.*, decreasing lifetimes):

$$\begin{aligned}
&\bullet\ 3 \to 6 \to 10 \to 15 \to \text{GS} \\
&\bullet\ 4 \to 8 \to 13 \to \text{GS} \\
&\bullet\ 5 \to 9 \to 14 \to \text{GS} \\
&\bullet\ 7 \to 11 \to \text{GS}
\end{aligned} \tag{55}$$

where 'GS' signifies the ground state. It is therefore only an initial condition that determines which trajectory a given system ultimately follows.

Given these results, we can separate the vacua in our vacuum tower into three distinct regions on the basis of their decay phenomenologies. This is illustrated schematically in Fig. 27. At the top of the tower is a stable region within which all vacua have lifetimes longer than the current age of the universe. This stable region is then separated from the remaining unstable regions by a "Great Wall" which denotes the border between the stable "civilized" world and the remaining "barbarian" regions which are afflicted with the omnipresent threat of sudden and spontaneous vacuum decay. Moving past the Great Wall, the second region is a cascade region in which there develops a complex pattern of decays of metastable vacua into other metastable vacua. Finally, moving further down the tower, the third region is a collapse region consisting of vacua which decay directly to the ground state of the theory.

Note that this last region may, in turn, be subdivided into two distinct (but overlapping) subregions. The first consists of vacua (such as the $n = \{11, 13, 14, 15\}$ vacua in the current example) which can be reached at the end of one or more decay chains beginning in the cascade region. By contrast, the second (which here technically includes the $n = 3, 4, 5, 7, 12$ vacua as well as all $n > 15$ vacua) consists of vacua which can never be reached through any instanton-tunnelling decay chain. These vacua, which may only be populated by some initial condition, collectively form a "Forbidden City" into which one cannot enter from the outside. Indeed, the universe can inhabit such a Forbidden City only if it was initially "born" there.

Thus, we see that constructions of this sort possess not only a great number of metastable vacua in addi-

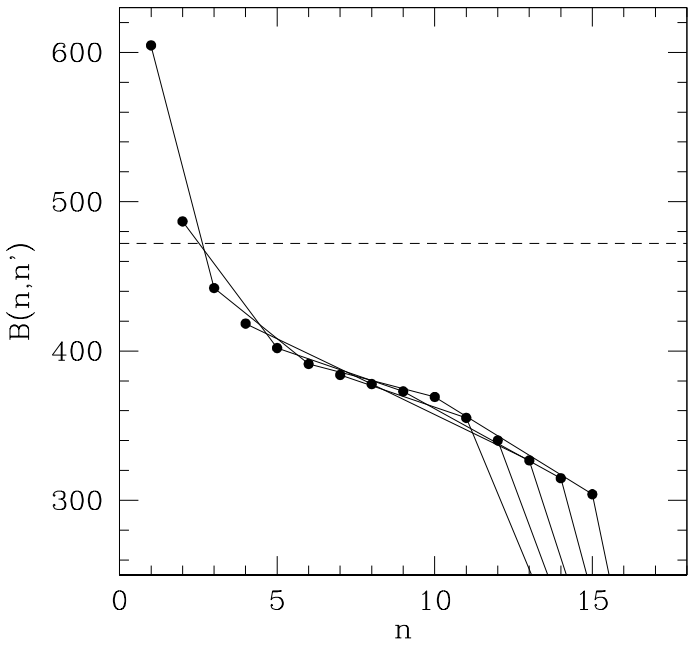

FIG. 26: Lifetimes along the different cascade trajectories, calculated for $N = 5000$ and $\chi = 2.8 \times 10^{-4}$. For each vacuum n, we plot $B(n, n')$ for that value of n' ($n < n' \leq N-1$) which minimizes $B(n, n')$ and which thereby indicates the next vacuum along the corresponding cascade trajectory. Points are connected according to their sequential trajectories. We also show the Great Wall (dotted line) signifying the critical bounce action corresponding to the age of the universe. We see from this plot that in this case the top two vacua are stable, while the $n = 3$ through $n = 10$ vacua cascade down along four distinct trajectories with decreasing lifetimes until they pass the $n = 11$ vacuum. At this stage, each trajectory decays directly to the ground state of our vacuum tower. By contrast, vacua beyond the $n = 15$ vacuum populate a "Forbidden City": it is impossible to tunnel into these vacua from any other locations along the vacuum tower, and the universe can inhabit such a vacuum (for a brief time only) if and only if it is initially born there.

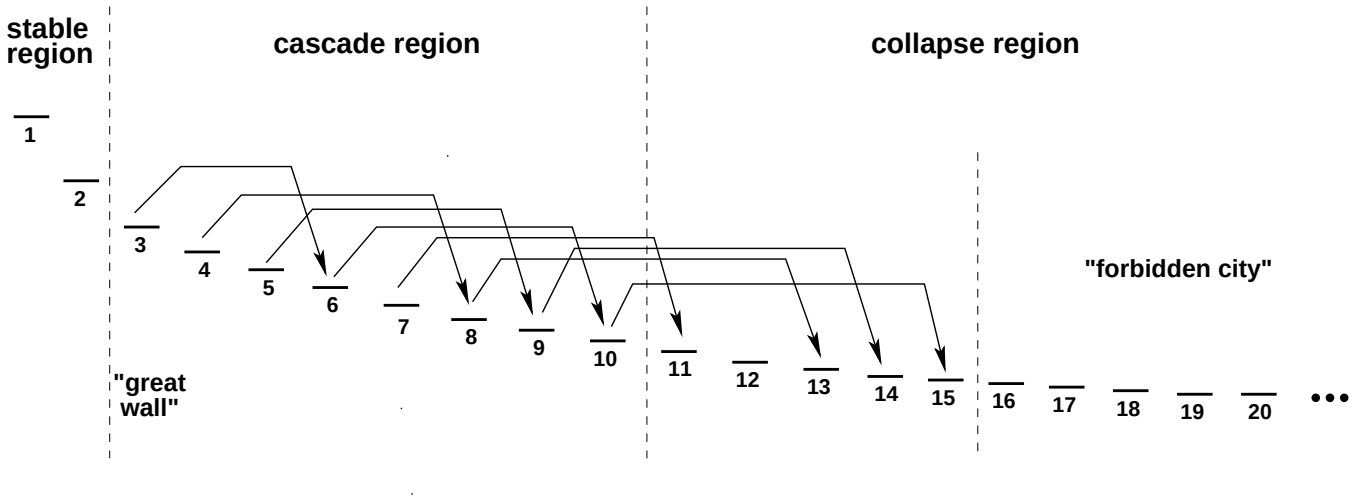

FIG. 27: A schematic of the vacuum structure of the model shown in Fig. 26. Vacua in the stable region to the left of the Great Wall have lifetimes exceeding the age of the universe, while vacua in the cascade region decay to other (lower) metastable vacua in the vacuum tower. By contrast, vacua in the collapse region decay directly to the ground state of the vacuum tower. Finally, vacua which populate the "Forbidden City" cannot be reached from outside the Forbidden City: such vacua can be populated only as an initial condition at the birth of the vacuum configuration.

tion to their ground states, but also the potential for a highly nontrivial set of vacuum dynamics involving complicated vacuum cascade/collapse behavior. In this vein, it is worth emphasizing that the example illustrated in Figs. 26 and 27 represents only one of many possible vacuum-cascade scenarios that can be realized in scenarios of this sort. Furthermore, if we were to relax some of the simplifying assumptions inherent in the model outlined in Section II — for example, our assumption that all nearest-neighbor kinetic-mixing parameters in Eq. (3) are equal, with all others vanishing — an even wider range of possible cascade scenarios would result. A similar possibility exists if λ is not taken in the asymptotic region: decreasing λ tends to decrease the lifetimes of our metastable vacua, and thereby enables more rapid vacuum transitions to occur.

IV. SPECTRUM OF THE MODEL

We now turn to a discussion of the spectra of physical particles that arise in the different vacuum states of our model. Rather than provide a detailed phenomenological analysis of these particles, our main interest is in understanding how their mass spectra evolve as functions of the vacuum index n. This will enable us to trace the changes in these particle spectra as our system evolves down the vacuum tower towards the ground state.

A. Scalar spectrum

We begin with the scalar sector, which comprises $2N+2$ degrees of freedom: the real and imaginary components of the ϕ_i. In any given vacuum, the squared masses of these states are the eigenvalues of the mass matrix defined in Eq. (11), with all fields replaced by their expectation values appropriate for that vacuum. However, we immediately observe from Eq. (30) that $N-1$ of the ϕ_i receive nonzero VEV's in any vacuum state. As a result, $N-1$ global $U(1)$ symmetries (corresponding to global phase rotations of these fields) are spontaneously broken, and we expect the spectrum to contain $N-1$ Nambu-Goldstone bosons. Thus $N-1$ of the eigenvalues of Eq. (30) will vanish, and the squared masses for the remaining $N+3$ scalar degrees of freedom will be positive (by definition, since each vacuum is presumed stable). Moreover, in any n-vacuum, four of these remaining $N+3$ degrees of freedom are the real and imaginary components of the two complex scalars ϕ_{N-n+1} and ϕ_{N+1} — the fields whose VEV's vanish in that vacuum — with masses proportional to $\lambda^2\xi^{N-1}$. The other $N-1$ degrees of freedom are real scalar fields (the real components of the ϕ_i for which $v_i^2 \neq 0$), and will have squared masses proportional to ξ.

B. Gauge-boson spectrum

As we have noted above, $N-1$ of the N different $U(1)$ gauge-group factors in our model are spontaneously broken in each vacuum state by the VEV's of the ϕ_i fields. As a result, the $N-1$ Nambu-Goldstone scalar modes discussed above are "eaten" by the gauge bosons associated with these broken $U(1)$'s, resulting in a gauge-boson mass matrix of the form

$$(M^2_{\rm gauge})_{ab} \;=\; g^2 \sum_i^{N+1} \hat{Q}_{ai}\hat{Q}_{bi}\, v_i^2 \;. \tag{56}$$

Here we have explicitly written the hats on the charge matrices, as in Sect. II, to indicate that they are defined in the basis in which gauge-kinetic terms take their canonical forms. Of course, this matrix (and indeed the physical mass spectrum dictated by its eigenvalues) is different for each vacuum in the tower. However, for all n, it has precisely one zero eigenvalue which corresponds to the linear combination of gauge bosons associated with the single remaining unbroken $U(1)$ gauge group. This linear combination, which we will call $U(1)'$ with gauge field B_μ, turns out to be a uniform admixture of the gauge fields $A^\mu_{N-n+1},\ldots,A^\mu_N$ in the *unhatted* basis:

$$B^\mu \;=\; \frac{1}{\sqrt{n}} \sum_{a=N-n+1}^{N} A^\mu_a \;. \tag{57}$$

Note that this massless gauge boson couples only to the complex scalars ϕ_{N-n+1} and ϕ_{N+1}.

The other $N-1$ linear combinations of gauge fields are nothing but massive Z' vector bosons with masses proportional to ξ (and independent of λ). Note that the mass of each such gauge boson is identical to that of one of the $N-1$ real, massive scalars mentioned above. This occurs because all non-vanishing quartic couplings among the various ϕ_i are given (in the unhatted basis) by g^2. This results in the massive gauge bosons having the same masses as the massive scalars. Indeed, such a situation arises as a result of the structure of the D-term potential in any supersymmetric theory in which there is no F-term contribution to the quartic couplings of the scalars.

C. Fermion spectrum

We now turn to the fermions in our model. These consist of the superpartners ψ_i of the complex scalars ϕ_i ($i=1,...,N+1$), as well as the gauginos λ_a associated with the $U(1)_a$ gauge groups ($a=1,...,N$). As a result, the fermion sector of the theory contains a total of $2N+1$ Weyl spinor degrees of freedom.

Since supersymmetry is broken in each vacuum in the tower, one of these spinors must play the role of the Goldstino. Moreover, since supersymmetry is broken solely

by D-terms in each vacuum, we can identify this particle with the gaugino superpartner of B^μ in Eq. (57). In supergravity scenarios, this particle is "eaten" by the gravitino according to the super-Higgs mechanism.

All other fermions are physical and acquire Dirac masses. In the n vacuum, we find that ψ_{N-n+1} and ψ_{N+1} (the superpartners of ϕ_{N-n+1} and ϕ_{N+1}) acquire masses proportional to $\lambda\xi^{(N-1)/2}$, stemming from superpotential contributions. The rest of the fermions acquire masses through terms of the form $\sqrt{2}v_i Q_{ai}\psi_i\lambda_a + \text{h.c.}$ that arise from the supersymmetrization of the gauge interactions, and the mass eigenstates of this latter group are often highly mixed.

D. Evolution of spectra under vacuum transitions

Given these results, we now seek to understand how these different mass spectra evolve as our system undergoes vacuum transitions from one vacuum to the next. In order to do this, it will be convenient to separate the physical, massive particles in the theory into two distinct classes based on whether they do or do not couple to the massless gauge field B^μ in Eq. (57).

As we have already seen, the particles which couple to B^μ are the component fields associated with the two chiral superfields Ψ_{N-n+1} and Ψ_{N+1}. These particles have masses proportional to $\lambda\xi^{1-N/2}$ and mix only with each other. Because these states couple to our only massless gauge boson B^μ in the theory, we shall refer to such states as "couplers".

By contrast, the remaining states in the theory couple only to the extra, massive Z' gauge bosons which are orthogonal to B^μ. As such, they do not couple to the massless gauge field B^μ itself, and we shall refer to these states as "non-couplers". These states are massive and highly mixed, with masses and mixings which are rather complicated functions of χ. Broadly speaking, however, these masses fill out a closely-spaced "band" which approaches a continuum as $N \to \infty$. Note that the masses of the non-couplers are λ-independent.

To help illustrate these features, let us consider the spectra of scalars and fermions that arise for the parameter assignments $N = 20$, $\chi = 1/4$, and $\lambda = \lambda^*_{20} \approx 1.05 \times 10^8$. These scalar and fermionic spectra are shown in Figs. 28 and 29, respectively. In each plot, the masses of the "coupler" fields are indicated by the solid curves. By contrast, the minimum and maximum masses of the remaining fields are indicated by dashed lines, and the spectral "band" of masses which they demarcate has been shaded.

These figures highlight several significant features of the particle spectra. First, it is evident from these figures that the masses of the couplers are highly dependent on the choice of vacuum. *In particular, it is the lightest coupler whose mass vanishes and then becomes tachyonic when a given vacuum is destabilized.* In this particular example, λ has been set to the critical value λ^*_{20}. Since

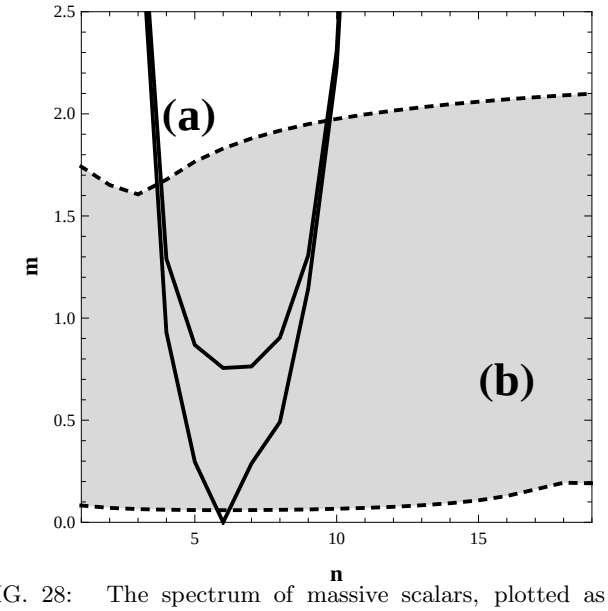

FIG. 28: The spectrum of massive scalars, plotted as a function of the vacuum index n for $N = 20$, $\chi = 1/4$, and $\lambda = \lambda^*_{20} \approx 1.05 \times 10^8$. (a) The solid lines indicate the masses of the two complex scalar "couplers", while (b) the dotted lines demarcate the edges of the shaded band within which the masses of the remaining scalars lie. Note that the lighter coupler actually becomes massless for the $n = 6$ vacuum; it is in this manner that the $n = 6$ vacuum begins to destabilize for $\lambda = \lambda^*_{20}$, in accordance with the results shown in Fig. 12 for $\chi = 1/4$. Note that the masses plotted are dimensionless rescaled masses, as discussed in Sect. II.

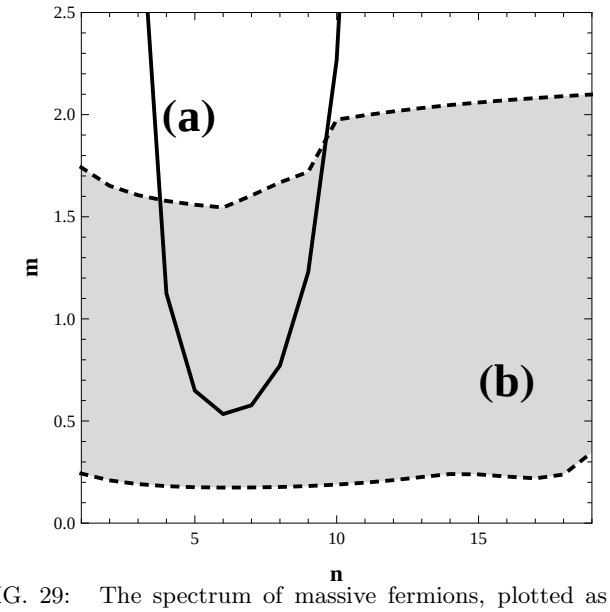

FIG. 29: The spectrum of massive fermions, plotted as a function of the vacuum index n for $N = 20$, $\chi = 1/4$, and $\lambda = \lambda^*_{20} \approx 1.05 \times 10^8$. (a) The solid line indicates the single fermionic "coupler", while (b) the dotted lines demarcate the edges of the the shaded band within which the masses of the remaining fermions lie. As in Fig. 28, the masses plotted are dimensionless rescaled masses discussed in Sect. II.

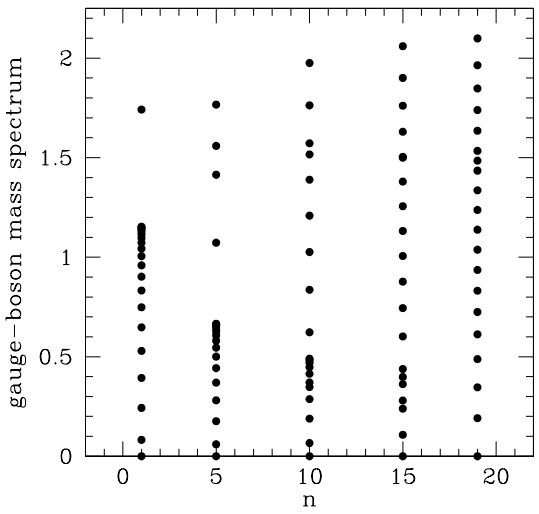

FIG. 30: Gauge-boson mass spectra, plotted for the $n = \{1, 5, 10, 15, 19\}$ vacua. For this plot, we have taken $N = 20$ and $\chi = 1/4$, and the (rescaled) masses are displayed on the vertical axis. Note that when n is small, many of the masses tend to cluster around a particular value. As n increases, however, this value drops; fewer of the masses are clustered around this value, and the masses of the remaining gauge bosons become more widely spaced. By contrast, the mass of the lightest massive gauge boson increases with increasing n. Thus, as our system tumbles down the vacuum tower, the lightest non-zero gauge boson tends to become increasingly heavy.

$\chi = 1/4$, we see from Fig. 12 that it is the $n = 6$ vacuum which is destabilized at this value of λ, and hence it is in the $n = 6$ vacuum that the lightest coupler becomes massless for this choice of parameters. By contrast, the other vacua near the top and bottom of the vacuum tower are more comfortably stable for this value of λ. As a result, the masses of the coupler fields become quite large for these vacua.

The situation is quite different for the non-coupler fields. For these fields, we see from Figs. 28 and 29 that the boundaries of the non-coupler spectral band remain roughly constant as one transitions from vacuum to vacuum. However, it will be noted that both the width of the band and the mass of the lightest particle in it increase slightly when n is near $N - 1$. It is also apparent from these diagrams that the lightest massive particles in any particular vacuum are generally the lightest non-coupler scalar and the lightest massive gauge field, both with precisely the same mass.

Figs. 28 and 29 are calculated for λ sitting precisely at the critical value λ^*_{20}. However, it is easy to see what happens as we increase λ: the solid curves corresponding to the coupler masses rescale with λ, while the shaded bands corresponding to the non-coupler masses remain invariant.

It is important to note that although the maximum and minimum of the non-coupler "bands" in Figs. 28 and 29 remain roughly constant as a function of vacuum index n, there nevertheless exists a rich n-dependence for the masses of the individual states within the band. This is shown in Fig. 30 for the gauge-boson spectrum. When n is small, many of the gauge-boson masses tend to cluster around a particular value. As n increases, however, the masses of the remaining gauge bosons becomes more widely spaced. By contrast, the mass of the lightest massive gauge boson increases with increasing n. Thus, as our system tumbles down the vacuum tower, the lightest non-zero gauge boson tends to become increasingly heavy.

Given these results, several intriguing phenomenological possibilities emerge. As we have seen, for any vacuum in our metastable vacuum tower, there is only one physical, massless field: this is the gauge boson in Eq. (57), associated with the single remaining unbroken $U(1)'$ gauge group. If this $U(1)'$ gauge boson resides in a hidden sector — or if it is identified with the photon — there should be no difficulties in making this model compatible with present experimental observations. In particular, if we imagine that all of our broken $U(1)$'s are hidden or broken at mass scales which exceed accessible energies, then only the coupler fields will be readily observable. Since the masses of these fields scale linearly with λ, we can easily adjust them to be unobservable as well. Thus, the presence of such large numbers of fields need not necessarily pose phenomenological difficulties.

On the other hand, it remains true that the spectrum contains a large number of massive gauge bosons, scalars, and Dirac fermions whose properties depend on the particular vacuum state in question. If such states are observable, such a spectrum could lead to a rich and interesting phenomenology, with a variety of potential implications for both collider physics and cosmology.

V. DEGENERATE VACUA AND BLOCH WAVES

Thus far, we have analyzed our model in the range $0 < \chi < 1/2$, and investigated the vacuum towers and tunnelling dynamics which result. Indeed, each successive vacuum in the tower has a lower energy than the previous one, and consequently there exists a net direction for dynamical flow.

All of this changes, however, if we consider the endpoint where $\chi = 1/2$. Note from Fig. 1 that for any N, the point at which χ is strictly equal to $1/2$ is still within our set of allowed values of χ. In this case, we find that $R_n = 2$ for all n, and the expressions for the vacuum energies V_n and saddle-point energies $V_{n,n'}$ become independent of their vacuum indices n, n'. As a result, the vacuum structure in the asymptotic-λ regime discussed in Sect. II consists of $N - 1$ *degenerate* vacua with energies $\langle V_n \rangle = 1/2$ for all n. These in turn are separated

from each other by a set of equivalent, saddle-point potential barriers of uniform height $\langle V_{n,n'}\rangle = 2/3$ for all n, n'. Furthermore, when $\chi = 1/2$, we find that the field-space configurations for our vacua and saddle points in Eqs. (30) and (32) respectively become essentially identical, differing from one another only insofar as a different VEV is set to zero in each case. This implies that the field-space distance between any pair of vacua is equal to that between any other such pair.

This behavior is shown in Fig. 31, where we plot the vacua and saddle points of our vacuum towers as a function of χ. For $\chi < 1/2$, we see that our vacuum tower "staircase" has a non-zero slope. However, as $\chi \to 1/2$, this slope becomes less and less until our vacuum tower becomes degenerate, with all vacua and saddle points having equal energies and distances in field space. This situation is shown in Fig. 31(c).

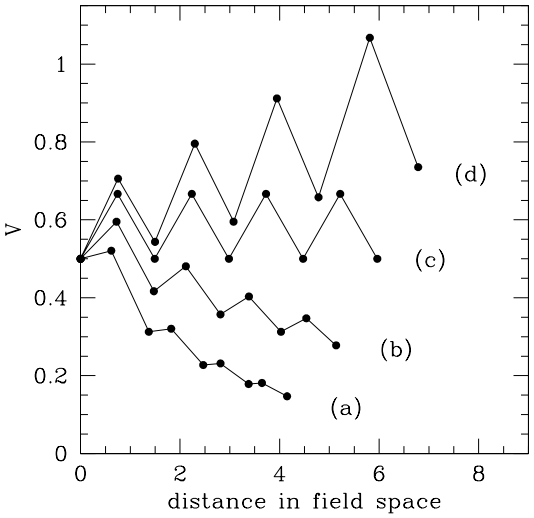

FIG. 31: Vacuum structure in the $N = 6$ model, plotted for (a) $\chi = 0.2$, (b) $\chi = 0.4$, (c) $\chi = 0.5$, and (d) $\chi = 0.54$. As χ increases from zero, we see that the "slope" of our vacuum "staircase" decreases, ultimately becoming completely flat at $\chi = 0.5$. For $\chi > 0.5$, the vacuum staircase inverts, with the lightest states now becoming the heaviest states.

Taken together, these results imply that that the transition rates between all vacua in the "tower" are identical for $\chi = 1/2$. As a result, all vacuum transitions in this setup will occur with identical rates, and it is no longer appropriate to employ the classical approximations discussed at the beginning of Sect. III in which we assume that only one decay channel dominates the tunneling dynamics. Instead, our system must be treated quantum-mechanically.

The result, however, is clear: the true ground state of such a theory is no longer any of the individual n-vacua by itself. Instead, what results is an infinite set of *Bloch waves* across the entire set of degenerate vacua. Moreover, the vacuum energies associated with such Bloch waves fill out a continuous band. As a result, the vacuum energy of the true ground state of the theory will be smaller than the vacuum energy of any individual vacuum.

The phenomenological implications of such a Bloch-wave vacuum structure will be discussed in more detail in Ref. [8]. Nevertheless, it is interesting to speculate that the vacuum energy of this true ground state might actually vanish. If this is possible, we would have a situation in which our Bloch-wave vacuum structure actually *restores* supersymmetry. Another possibility is that the vacuum energy of this true ground state only *approaches* zero as $N \to \infty$. In this case, one could potentially obtain a ground state with a very small cosmological constant, in a manner reminiscent of the proposal in Ref. [5]. These and other issues will be explored more fully in Ref. [8].

Needless to say, the existence of such Bloch-wave ground states is yet another example of a non-trivial vacuum structure associated with the moose. In some sense, the "translational" symmetry that shifts us from one degenerate vacuum to the next is nothing but a reflection of the underlying translational symmetry of the original moose. We caution, however, that it is not merely *any* moose which gives rise to this sort of band structure; it is only one with a precise value for the kinetic mixing between nearest-neighbor $U(1)$ gauge factors, as well as non-trivial Fayet-Iliopoulos terms. Together, it is these ingredients which conspire to produce a vacuum structure consisting of an infinite number of degenerate vacua, each of which is stable (lacking either tachyonic or flat directions), with a non-zero transition probability between them. However, once these features are achieved, the ensuing Bloch-wave vacuum structure is inevitable.

VI. DISCUSSION

In this paper, we have presented explicit examples of two new highly non-trivial vacuum structures that can arise in supersymmetric field theories. In particular, we have shown that when kinetic mixing among its $U(1)$ gauge groups is permitted, an N-site Abelian moose construction gives rise to a tower of $N-2$ metastable vacua, each of which involves nonzero VEVs for all but two of the "link" fields on the moose, in addition to a stable ground state. As N is increased, the energies of the existing vacua remain unchanged, while new vacua appear with smaller and smaller energies, the lowest of which asymptotically approaches zero as $N \to \infty$. We investigated the dynamics associated with transitions between these vacua, and found that different regions of the vacuum tower could manifest very different instanton-induced vacuum-decay patterns. These include "collapse" regions, in which all vacua decay directly to the ground state in a particular order; "cascade" regions, in which a potentially complicated decay chain from metastable vacuum to metastable vacuum develops; stable regions in which the vacuum states have lifetimes exceeding cos-

mological time scales; and regions into which instanton-induced tunnelling cannot occur. We also explored the particle spectra associated with these vacua, and showed that in each vacuum state there exists only one physical, massless mode — the gauge boson associated with the lone unbroken $U(1)$ in that vacuum — along with a tower of massive gauge bosons, scalars, and Dirac fermions. The massless state is coupled to the rest of the states in the tower only by highly-suppressed interactions involving extremely heavy particles, and thus can be viewed as part of a decoupled hidden sector.

Needless to say, there are many additional avenues through which additional properties of our model might be explored. For example, we have already seen in Sect. V that the $\chi \to 1/2$ limit of our general framework produces a Bloch-wave structure for the true ground state of the theory. This is another unique vacuum structure which has not been explored in the literature thus far, but which clearly emerges in models of this type. Models exhibiting Bloch-wave ground states can be expected to have phenomenologies which differ markedly from those based on single vacuum states, much as the strong CP problem of QCD is a feature uniquely associated with the QCD θ-vacuum. A detailed examination of the implications of such a vacuum structure is forthcoming [8].

Another salient issue worthy of investigation concerns the *thermal* properties of such an infinite tower of metastable vacua. In this connection, there are two issues which are of paramount importance: that of initially populating the landscape, and that governing its decay patterns.

The former issue is critical for determining whether the universe tends to start out in the cascade region near the top of the tower, in the collapse region near the middle of the tower, or at the bottom, at or near the ground state. Broadly speaking, vacua which contain more light degrees of freedom tend to be preferred in a thermal context. Occasionally, this means that the universe is far more likely to end up in a metastable state than in the ground state of a given theory. In the scenarios discussed in Ref. [2], for example, it is has been shown [21] that thermal effects prefer the metastable vacuum. By contrast, in our model, the number of light degrees of freedom in any given vacuum along the tower is essentially vacuum-independent. Thus it is not *a priori* obvious into which vacuum state the universe would prefer to settle, or whether a (potentially large) number of states would emerge as equally likely candidates. This would be an interesting area for future research.

The latter issue is also extremely important, for in this paper we have limited our attention to vacuum decays which proceed through instanton-induced tunneling. While this is indeed the whole story at zero temperature, finite-temperature scenarios contain additional *sphaleron*-like processes through which such vacua might also decay. This has the potential to significantly modify the vacuum dynamics we discussed in Sect. III. For example, while the Forbidden City cannot be entered through instanton-tunnelling transitions, it can nevertheless be entered through thermal excitations.

A final question worth exploring concerns the theoretical interpretation of our model. As we have seen in Sect. II, our model has as its core an N-site moose theory of a sort which is familiar to deconstructionists [22]. This suggests that our model should have a natural five-dimensional interpretation in the $N \to \infty$ limit. However, our moose theory is complicated by the fact that we must introduce non-zero kinetic mixings between nearest-neighbor $U(1)$'s in order to achieve vacuum stability. One wonders, then, about the extent to which this modifies our previous five-dimensional interpretation. One possible clue comes from the fact that we can "rotate" our $U(1)$ basis in such a way as to eliminate the kinetic mixing entirely; this occurs at the cost of introducing three or more non-zero $U(1)$ charge assignments for each of our chiral superfields as well as the introduction of non-zero "bulk" Fayet-Iliopoulos terms which are located off the moose endpoints. In general, it is known [23] that introducing non-uniform gauge charges along the moose is one way of realizing warped or other non-trivial geometries. It therefore remains to be seen which, if any, warped five-dimensional geometry might effectively emerge from our model in the $N \to \infty$ limit. This could be important for understanding the set of possible UV completions of our model. Indeed, some of these completions might also potentially include gravitational effects, as have been considered in other metastable models [13, 24],

Clearly, there are also a number of possible applications for a vacuum structure of this sort.

Perhaps the application which most immediately springs to mind concerns a potential solution to the cosmological-constant problem. Over the past decade, several scenarios have been proposed in which a small cosmological constant emerges as a consequence of a large number of vacua [3, 4, 5, 6]. Scenarios of this sort tend to posit the existence of a "landscape" of vacua with certain gross properties, including a vacuum state whose energy is nearly vanishing. One then imagines that the universe either dynamically tumbles down to this special vacuum state, or is somehow born there.

However, to the best of our knowledge, no explicit model with a vacuum structure exhibiting such properties has ever been constructed. Moreover, most of the existing scenarios have been proposed in the context of the string-theory landscape, where the different vacua correspond not to different minima of the same theory, but to separate theories characterized by distinct parameter assignments, gauge structures, particle contents, *etc*. In such a context, it is not clear that the instanton methods of Ref. [25] apply. In fact, it is not at all obvious how (or even if) transitions between models can occur in such a framework. As a result, it is not clear how the landscape of vacua can be populated even qualitatively, much less quantitatively.

By contrast, the towers of metastable vacua in our model exist at a single point in parameter space — that

is, for a single choice of χ, ξ, M, and λ — and correspond to different vacuum states *within the same theoretical model*. The method by which transitions occur between one vacuum state of the theory and another is therefore well understood, both at zero temperature and at finite temperature. As a result, reliable statements can be made concerning both the initial, statistical population mechanism for these vacua as well as the dynamics associated with transitions between them.

Regardless of the particular scenario envisioned, it is important to note that a solution to the cosmological-constant problem requires not only a small energy for the vacuum we inhabit, but also that the additional particles present in the model be thus far experimentally observable. Thus, either the masses of all additional particles appearing in that particular vacuum must be heavy enough to have thus far avoided detection, or else these additional fields must decouple from those of the Standard Model and form a hidden sector. Whether the former criterion is met in any given vacuum depends sensitively on the values of our underlying model parameters.

It is also important to note that we can achieve a true ground state with nearly vanishing vacuum energy only by fine-tuning the parameter N in our model. Specifically, if we wish our ground state to have a very small vacuum energy, we will require a large number of sites on the moose. This is not surprising, since we cannot expect to have a fine-tuned ground state without introducing our fine-tuning in some other fashion. Indeed, while most previous scenarios merely posit a large number of vacua as an initial condition for obtaining a small cosmological constant, we are explicitly realizing this large number of vacua as the result of a different, equally large number: the number of $U(1)$ gauge factors in an underlying moose. However, we stress that this is a relatively small price to pay, since we are obtaining a calculable tower of metastable vacua in the process, each of which is free of both tachyonic and flat directions, along with a true, stable ground state with the small vacuum energy we desire.

There are other potential applications of our model as well. For example, one of the major thrusts in recent string-theoretic research has been a statistical study [26] of the string landscape [27]. Through such statistical studies, one hopes to uncover hidden correlations which may be taken as predictions from (or evidence of) an underlying string structure at high energy scales. However, one important issue that needs to be addressed in this context concerns the proper definition of a *measure* across the landscape: in what manner are the different string theories to be weighted relative to each other? Clearly, the most naïve approach is to count each string model equally, interpreting each as contributing a single vacuum state to the landscape as a whole. However, it is entirely natural that moose theories of the sort we have been examining in this paper can appear as the actual low-energy (deconstructed) limits of flux compactifications [13], and as we have seen, such theories give rise to infinite towers of metastable vacua. Indeed, for certain choices of the underlying parameters in these models, literally all of these vacua may be rendered stable on cosmological time scales. The question then arises as to whether such theories should be weighted according to the infinitely large number of vacua which they contribute to the landscape as a whole. In fact, following this line further, it becomes crucial to determine whether the landscape measure should be defined in terms of different *theories*, or in terms of the different *vacua* they contain. Indeed, if the true underlying landscape measure is based on vacua, then a theory with infinite towers of vacua is likely to dominate any statistical study of the string landscape. As such, the phenomenological properties of these sorts of models will dominate the properties of the landscape as a whole.

Another potential application of the model described here is as a possible hidden sector in a fully developed model of supersymmetry breaking. The advantage of this would be that a hierarchy between the Planck scale and the supersymmetry-breaking scale could arise dynamically, as a consequence of vacuum tumbling dynamics along the tower. In order for this to be viable, however, a number of phenomenological issues would need to be addressed. For example, while supersymmetry is indeed broken in each vacuum state in the tower, it is broken only by background values for the D-terms associated with the various $U(1)$ gauge groups in the model. Consequently, R-symmetry is left unbroken in each vacuum. If the dominant source of supersymmetry-breaking is to come from a sector of this sort, then the introduction of additional matter will be required in order to obtain realistic masses for the gaugino superpartners of the Standard-Model gauge fields. Likewise, it is possible that an F-term component to supersymmetry breaking could be engineered via a a modification of this scenario to include additional, vector-like matter in a manner similar to that discussed in Ref. [14].

Needless to say, these are only some of the many applications such a vacuum structure might have. There exist, however, numerous additional possibilities. For example, because our construction relies directly on the presence of extra $U(1)$ gauge symmetries, the low-energy limit of our setup could have significant implications for Z' phenomenology. Indeed, if the coupling between our setup and the Standard Model is properly engineered, the collider signatures of such a scenario could be rather dramatic. Note that preliminary analyses of the mass spectra associated with each vacuum in the tower can be found in Sect. IV.

Likewise, this scenario could also have a number of astrophysical and cosmological implications. The vacuum cascade we have discussed in Sect. III involves numerous first-order phase transitions, and is therefore likely to generate topological defects. In particular, given that our model contains numerous Abelian gauge factors, there is a specific likelihood of generating a network of cosmic strings [28]. Moreover, different regions of the universe

could potentially exist in different vacuum states along the tower, giving rise to domain walls. It therefore becomes an important phenomenological question as to how the constraints associated with such domain walls might be alleviated.

In summary, then, it is clear that a number of potential extensions and applications exist for the new vacuum structures presented in this work. Indeed, as the poet William Carlos Williams might well have written,

```
So much depends
upon

the vacuum
structure

glazed with
excitations

forming white
chickens. [29]
```

Acknowledgments

This work was supported in part by the Department of Energy under Grant DE-FG02-04ER-41298. We are happy to thank E. Dudas, T. Gherghetta, G. Shiu, and U. van Kolck for discussions. Moreover, for Great Walls and Forbidden Cities, there is nothing better than the real thing. We are therefore also delighted to thank the new Kavli Institute for Theoretical Physics (KITPC) in Beijing, China, for gracious hospitality, an excellent research environment, and abundant inspiration of Olympic proportions during the completion of this work. Long may she prosper!

[1] J. R. Ellis, C. H. Llewellyn Smith and G. G. Ross, Phys. Lett. B **114**, 227 (1982); M. Dine and A. E. Nelson, Phys. Rev. D **48**, 1277 (1993) [arXiv:hep-ph/9303230]; M. Dine, A. E. Nelson, Y. Nir and Y. Shirman, Phys. Rev. D **53**, 2658 (1996) [arXiv:hep-ph/9507378]; S. Dimopoulos, G. R. Dvali, R. Rattazzi and G. F. Giudice, Nucl. Phys. B **510**, 12 (1998) [arXiv:hep-ph/9705307]; M. A. Luty, Phys. Lett. B **414**, 71 (1997) [arXiv:hep-ph/9706554]; M. A. Luty and J. Terning, Phys. Rev. D **62**, 075006 (2000) [arXiv:hep-ph/9812290].

[2] K. Intriligator, N. Seiberg and D. Shih, JHEP **0604**, 021 (2006) [arXiv:hep-th/0602239]; JHEP **0707**, 017 (2007) [arXiv:hep-th/0703281].

[3] R. Bousso and J. Polchinski, JHEP **0006**, 006 (2000) [arXiv:hep-th/0004134]; J. L. Feng, J. March-Russell, S. Sethi and F. Wilczek, Nucl. Phys. B **602**, 307 (2001) [arXiv:hep-th/0005276].

[4] T. Banks, M. Dine and L. Motl, JHEP **0101**, 031 (2001) [arXiv:hep-th/0007206].

[5] G. L. Kane, M. J. Perry and A. N. Zytkow, arXiv:hep-th/0311152.

[6] See, *e.g.*, S. H. H. Tye, arXiv:hep-th/0611148; arXiv:0708.4374 [hep-th]; S. Sarangi, G. Shiu and B. Shlaer, arXiv:0708.4375 [hep-th].

[7] S. S. Haque, G. Shiu, B. Underwood and T. Van Riet, arXiv:0810.5328 [hep-th].

[8] K. R. Dienes and B. Thomas, to appear.

[9] M. B. Green and J. H. Schwarz, Phys. Lett. B **149**, 117 (1984).

[10] E. Dudas, A. Falkowski and S. Pokorski, Phys. Lett. B **568**, 281 (2003) [arXiv:hep-th/0303155].

[11] B. Holdom, Phys. Lett. B **166**, 196 (1986).

[12] K. R. Dienes, C. F. Kolda and J. March-Russell, Nucl. Phys. B **492**, 104 (1997) [arXiv:hep-ph/9610479].

[13] K. R. Dienes, E. Dudas and T. Gherghetta, Phys. Rev. D **72**, 026005 (2005) [arXiv:hep-th/0412185].

[14] K. R. Dienes and B. Thomas, Phys. Rev. D **78**, 106011 (2008) [arXiv:0806.3364 [hep-th]].

[15] M. T. Grisaru, W. Siegel and M. Rocek, Nucl. Phys. B **159**, 429 (1979).

[16] S. Weinberg, Phys. Rev. Lett. **80**, 3702 (1998) [arXiv:hep-th/9803099].

[17] A. Falkowski, C. Grojean and S. Pokorski, Phys. Lett. B **581**, 236 (2004) [arXiv:hep-ph/0310201].

[18] U. van Kolck, Nucl. Phys. A **645**, 273 (1999) [arXiv:nucl-th/9808007]; P. F. Bedaque and U. van Kolck, Ann. Rev. Nucl. Part. Sci. **52**, 339 (2002) [arXiv:nucl-th/0203055].

[19] S. R. Coleman, Phys. Rev. D **15**, 2929 (1977) [Erratum-ibid. D **16**, 1248 (1977)]; C. G. . Callan and S. R. Coleman, Phys. Rev. D **16**, 1762 (1977).

[20] M. J. Duncan and L. G. Jensen, Phys. Lett. B **291**, 109 (1992).

[21] S. A. Abel, C. S. Chu, J. Jaeckel and V. V. Khoze, JHEP **0701**, 089 (2007) [arXiv:hep-th/0610334]; N. J. Craig, P. J. Fox and J. G. Wacker, Phys. Rev. D **75**, 085006 (2007) [arXiv:hep-th/0611006]; W. Fischler, V. Kaplunovsky, C. Krishnan, L. Mannelli and M. A. C. Torres, JHEP **0703**, 107 (2007) [arXiv:hep-th/0611018].

[22] N. Arkani-Hamed, A. G. Cohen and H. Georgi, Phys. Rev. Lett. **86**, 4757 (2001) [arXiv:hep-th/0104005]; C. T. Hill, S. Pokorski and J. Wang, Phys. Rev. D **64**, 105005 (2001) [arXiv:hep-th/0104035].

[23] K. Sfetsos, Nucl. Phys. B **612**, 191 (2001) [arXiv:hep-th/0106126]; H. Abe, T. Kobayashi, N. Maru and K. Yoshioka, Phys. Rev. D **67**, 045019 (2003) [arXiv:hep-ph/0205344]; L. Randall, Y. Shadmi and N. Weiner, JHEP **0301**, 055 (2003) [arXiv:hep-th/0208120].

[24] Z. Lalak and O. J. Eyton-Williams, arXiv:0807.4120.

[25] J. D. Brown and C. Teitelboim, Phys. Lett. B **195**, 177 (1987).

[26] M. R. Douglas, JHEP **0305**, 046 (2003) [arXiv:hep-th/0303194].

[27] L. Susskind, arXiv:hep-th/0302219.

[28] H. B. Nielsen and P. Olesen, Nucl. Phys. B **61** (1973) 45; T. W. B. Kibble, J. Phys. A **9**, 1387 (1976).

[29] http://en.wikipedia.org/wiki/The_Red_Wheelbarrow